Potential volumes of arsenic in Holocene clay plug sediments in Bihar, India

By

Floortje Burgers

in partial fulfilment of the requirements for the degree of

Bachelor of Science
in Applied Earth Sciences

at the Delft University of Technology,
January 2017

Supervisors: Dr. M.E. Donselaar
Prof. Dr. J. Bruining

TU Delft

Abstract

Natural occurring arsenic contamination of shallow aquifer groundwater is a problem affecting millions of people worldwide. Long term exposure to high concentrations results in severe medical conditions. On-going research into the origin and spread of the problem, risk mitigation and problem solving is of great importance. Sediment eroded and transported from mountains adsorbs arsenic (As) from river water onto its iron oxyhydroxides coatings. The geomorphology of the river is related to the concentration of As in shallow aquifers. Helicoidal flow in a meandering river leads to erosion of the cut bank in the outer bend and accumulation of sediment at the point bar in the inner bend. The result is an asymmetrical depth profile. The process of meandering and avulsion sometimes leads to the complete abandonment of a part of the river's channel. This still-standing water body is known as an oxbow lake. Fine sediment settles from suspension and the oxbow lake gradually fills up with silt and clay. A clay plug forms, surrounding the sands of the adjacent point bar. Clay filled oxbow lakes formed by meandering rivers are high in organic content and the anoxic conditions in the hypolimnion are considered the source for the release of the adsorbed arsenic. Under reducing conditions the As is released from its solid state by microbial respiration. In the geomorphological setting of meandering rivers, abandoned channels and point bar, this process of reductive dissolution is the generally accepted release mechanism for arsenic.

This research aims to provide insight in the potential arsenic volume in Holocene clay plugs in Ganges River floodplains and to present ideas on the migration processes of arsenic from clay plug to adjacent point bar. Migration of dissolved As occurs by advection and by diffusion. Satellite data from Google Earth Pro was used to simulate clay plugs with a Matlab model. The simulated data was used for the calculations of the surface area of the clay plug, the volume of the clay plug, the potential volume of As and the contact area between the clay plug and adjacent point bar. These geometric properties and concentrations of As were used to apply Fick's first law to estimate the initial diffusion flux and the initial discharge.

The surface area of the twenty selected clay plugs vary from 10^5 to 10^7 m^2. The corresponding volumes are in the order of magnitude of 10^6 to 10^8 m^3. The calculated As volumes range within the orders of 10^5 to 10^6 kg. The initial diffusion flux was calculated and ranges approximately between 15-300 g/m^2year. For the volume calculations the exact shape of the depth profile turned out to be of little influence. For calculations of the contact area and thus the diffusion flux estimations, the true profile is crucial. In-situ sampling would provide data to minimize uncertainties and improve results.

Contents

Introduction

Pollution of groundwater by naturally occurring arsenic (As) is a problem affecting over 140 million people in at least 70 different nations (Ravenscroft, 2007). What was thought to be a local problem before is now globally recognised. In India and Bangladesh the pollution of drinking water with As in the Ganges-Brahmaputra-Meghna delta (GBM) was discovered in the 1980s (Bhattacharya, 1997; Ravenscroft, 2009) The World Health Organisation (WHO) spoke of the problem in Bangladesh as 'the largest poisoning of a population in history' (Smith et al., 2000). The recommended limit by the WHO for As in drinking water is 10 µg/L (WHO, 1993, 2011). Some countries such as Nepal, Bangladesh and India set the national standard at 50 µg/L. However, As concentrations in contaminated water far exceed these limits too (Uddin and Huda, 2011). Multiple studies report values of As >400 µg/L (Berg et al., 2001, Ravenscroft, 2009). Since the first report of As contamination of shallow aquifer groundwater many studies have been conducted to understand the extents of the problem. The source of the As, release mechanisms, migration processes and solutions to the problem are just a few subjects of the on-going research.

The geomorphological setting of the contaminated aquifer has been linked to the variability in As concentration. Three geomorphological features have been consistent throughout many studies (Donselaar et al. 2016). As concentrations have been high in aquifers of these elements; meandering river deposits, abandoned channel (oxbow lake) clay deposits and sandy point bar deposits. *Figure 1.1* shows the main morphological features of a meandering river. Under normal conditions, a river expands laterally over the floodplains due to meandering and avulsion. Helicoidal flow in the meandering river leads to accumulation of sediment up the point bar in the inner bend and erosion of the cut bank in the outer bend (Schumm, 1977). This results in a steep eroded slope in the outer bend and a gentle slope on the inner bend of the meander. Sometimes part of the channel is abandoned and completely cut off. Fine sediment settles from suspension in this still-standing water body and the lake gradually fills up with clay and silt. The clay filled oxbow lake forms a clay plug around the adjacent point bar sands. These clay plugs are high in total organic content and the anoxic conditions in the hypolimnion of the lake are considered the source for the release of arsenic.

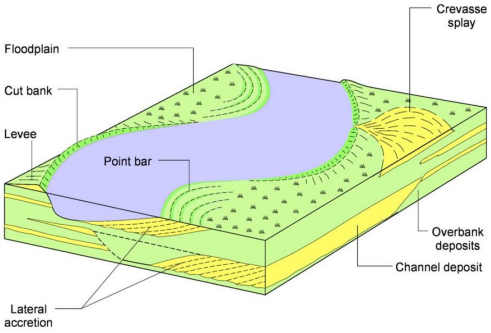

Figure 1.1: The major morphological features of a meandering river. From Nichols, 2009.

The problem is most severe in shallow aquifers of Holocene floodplains. Groundwater from shallow aquifers around Ganges River has been reported as highly contaminated by many studies. Concentrations of As in groundwater in the state of Bihar, India, far exceed the maximum considered safe (Chakraboti et al., 2003; BGS and DPHE, 2001). The highest contamination of As measured by Ghosh et al. (2007) is 1861 µg/L in the western district of Bhojpur. The objective of this research is to quantify the potential volume of arsenic released from recent clay plugs in Holocene Ganges River floodplains and to present ideas of the migration processes of dissolved arsenic to the adjacent point bar. A brief literature study on arsenic and its origin in the area of Bihar, India is conducted. Next, the dimensions and properties of twenty clay plugs are calculated. The volume of the clay plugs is simulated based on a depth profile and data from Ghosh et al. (2015) is used to quantify the As content in the clay plugs. After these calculations, a discussion and conclusions are provided, from which recommendations for future studies follow.

Area of study

Bihar is one of 36 states and union territories of the Republic of India. The state is divided in 38 administrative districts and each district is further divided into blocks. According to the 2011 census Bihar's population is over 103 million. Nearly 89 percent of the people live in rural areas. Multiple studies reported arsenic pollution groundwater in several districts in Bihar. These districts are Begusarai, Bhagalpur, Bhojpur, Buxar, Darbhanga, Katihar, Khagaria, Kishanganj, Lakhisarai, Munger, Patna, Purnea, Samastipur, Saran and Vaishali (Saha, 2009; Bhattacharya et al., 2011; Ghosh, 2015; Chakraboti et al., 2016). Bihar borders Uttar Pradesh in the west, West Bengal in the east and Jharkand in the south. In the north the state borders Nepal. The state stretches out in front of the Himalayas and lies on the vast alluvial plains of the Ganges River. This chapter discusses the geological and geomorphological settings of Bihar.

Figure 2.1: Area of study, Bihar, India (black)

2.1 Geological setting

The Indian sub continent consists of three geological subdomains; the Himalaya, the Indo-Gangetic Plain (IGP) and Peninsular India. The IGP is the extensive alluvial plain of the Ganges, Brahmaputra and Indus rivers and their tributaries. The Indian Peninsula is separated from the Himalayas by the IGP. The central part of the IGP, stretching from New Delhi to Kolkata and nearly covering the northern part of India, is the Ganges Plain (Singh, 1996). *Figure 2.2* from Singh (1996) shows the Ganga Plain (A) within the IGP. Part of the Ganga Plain is the Ganges Basin, which an element of an active Himalaya foreland basin. According to DeCelles and Giles (1996) all main elements of a foreland basin are present. The components of a foreland basin are orogeny, deformed foreland basin deposits adjacent to the orogeny, a depositional basin and peripheral cratonic bulge. The Himalaya are the orogen, the Siwalik Hills are the deformed deposits, the Ganges Basin is the depositional basin and the Bundelkhand Plateau (south of Uttar Pradesh) is the cratonic bulge (Singh, 1996, Sinha et al., 2005). After the break up of supercontinent Pangea during the Jurassic, two continents were formed; Laurasia and Gondwana. The Thetys Ocean separated these continents. The Indian Continent was part of Gondwana and the Eurasia was part of Laurasia. Once the Indian Plate broke apart during the Late Cretaceous and Paleocene, it started moving rapidly north towards the Eurasian plate. The movement of the Indian Plate closed the Thethys Ocean that occupied the area in between the two plates. The on-going collision between the two plates also caused the Himalayan orogeny. In the Miocene the Ganges Basin was formed in response to the uplift of the mountains. The Indian Plate underthrusts the Eurasian Plate and the basin was defined when the compressive forces of the collision resulted in lithospheric flexure and thrust-fold loading led to subsidence (Powers et al., 1998). During the Middle Miocene to Middle Pleistocene the Siwalik Hills were formed. Thrust loading caused the northern part of the basin to uplift; it was forced towards the basin. This caused the Ganges Basin to shift to the south (Singh, 1996). The Ganges foreland basin is since the Pliocene dominated by river systems. Over time the high load of sediment has forced the Ganges River to progradate towards edge of the basin, where there is still space for the rivers to meander and deposit sediment. During the Quaternary alluvial

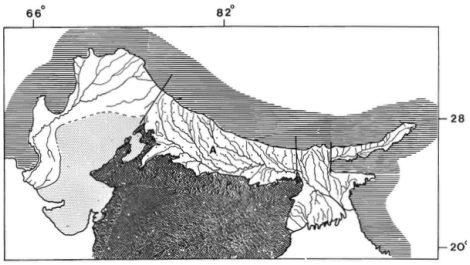

Figure 2.2: The Ganga Plain (A) shown within the Indoo-Gangetic Plain. From Singh (1996).

and fluvial sediments were deposited. Multiple transverse and oblique fault cross the Ganges Basin. Seismic data shows that many of these are active (Sinha et al., 2005).

2.2 Geomorphological setting

The Ganges River originates in the Himalaya and ends in the Bay of Bengal. It flows right through the Ganges Basin and several other rivers from both the Himalayas and Peninsular India join the river. The Brahmaputra River and the Meghna River are the main rivers to join. The three rivers together have formed one of the largest deltas in the world. This delta is known as the Ganges-Brahmaputra-Meghna (GBM) delta or the Bengal delta. The rivers carry high sediment loads and most sediment is deposited in the rivers' depositional basins. The remaining sediment is transported to the delta and deposited in a submarine fan-shaped body in front of the coast. The Bengal Fan is the largest submarine fan on earth and covers the bottom of the Bay of Bengal completely. Some of the other rivers joining the Ganges River in the area of Bihar are the Kosi River, the Gandak River and the Sone River. *Figure 2.3* shows the major rivers and some of their tributaries.

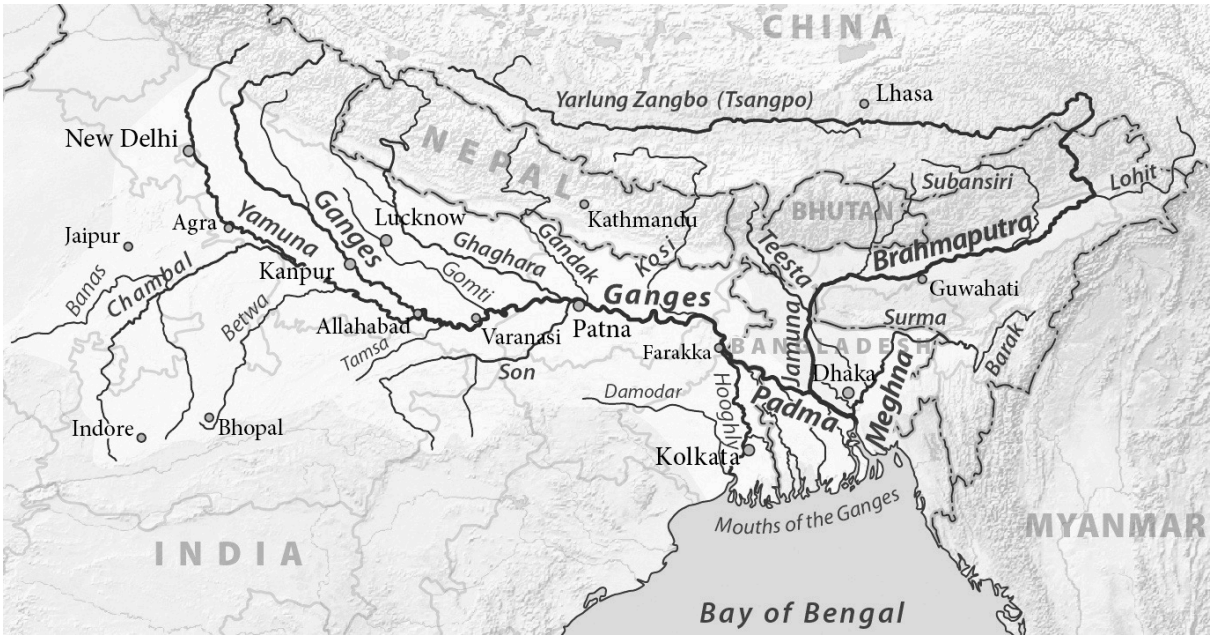

Figure 2.3: Overview of the major rivers and their tributaries of the Ganges-Brahmaputra-Meghna delta. After Wikimedia Commons.

There are three different types of fluvial systems; the division is based on the origin of the sediment load. Close to the origin in mountainous areas rivers are braided, multi channel rivers with a high sediment load. Once the area flattens and the gradient becomes lower, the rivers become meandering rivers. The third type of river is a smaller, single channel river with its origin in foothills or plains (Sinha and Friend, 1994). The Ganges, Kosi and Gandak Rivers are all mountain fed rivers because they enter the Ganges Plain from surrounding mountainous areas. They have high rates and high loads of sediment transport. Throughout the Ganges Plain the rivers meander until they reach the delta.

The fluvial system has different morphological features where sediment is deposited. First there are the vast floodplains, second there are the abandoned river channels and last there are point bars, adjacent to the abandoned channels. During flood periods the riverbanks overflow and water reaches the floodplain. Silt and clay settle from suspension and are deposited on these extensive plains. Under normal conditions, the rivers expand laterally due to meandering and avulsion. Meandering is the increase in sinuosity of the river path and avulsion is the formation of a new river course caused by levee breakthrough. The avulsion

and meandering sometimes result in the partial abandonment of a river channel. When completely cut off, the water in the abandoned river bend becomes a still-standing body: an oxbow lake. Fine sediment settles from suspension. The oxbow lake gradually fills up with clay and silt. Surrounding lacustrine plants and axonic conditions in the hypolimnion of the lake result in high organic carbon content and microbial respiration in the clay plug sediments (Donselaar et al., 2016). Helicoidal flow in the river results in the accumulation of sediment onto the point bar in the inner bend of the meander (Schumm, 1977) and erosion of the cut bank in the outer meander bend. The river path shifts and a migrating sand dune is formed. There is a decrease in energy up along the point bar slope, which leads to the deposition of finer sediment at the top. This results in a vertical fining upwards succession (Donselaar et al., 2016). During floods finer silt and clay sediments are deposited atop the point bar, forming impermeable boundaries along the point bar slope. The dynamics of the fluvial systems result in spatial varying deposits, sometimes overlaying each other. It is often suggested these oxbow lakes and clay plugs are the major sources for reactive organic matter and thus they are often associated with high concentrations of arsenic (Ravenscroft et al., 2001, McArthur et al., 2004, Nath et al., 2005). O

Arsenic

Natural and anthropogenic processes can introduce arsenic (As) into the groundwater. In different forms the element has many applications, and activities such as mining can mobilise geogenic As. The change of the controlling, reducing conditions causes the mobilisation of As (Brown et al., 2010). However it is naturally occurring and naturally mobilised As that causes major health risks worldwide. This chapter provides a brief chemical background on As and its toxicity, discusses the release system of reductive dissolution and discusses the migration processes of As.

3.1 Introduction to arsenic

Arsenic is the thirty-third chemical element and is considered a metalloid. It has three allotropes; gray, yellow and black (Norman, 1998). It occurs in nature in four oxidation states; -3, 0, 3 and 5. In groundwater As primarily occurs as arsenite As(III) and arsenate As(V). In soils both organic and inorganic forms occur. The inorganic forms are found as minerals whereas the organic forms occur in living organisms due to microbial respiration (Kossoff and Hudson-Edwards, 2012; Smith et al., 1998; Ghosh et al., 2015). Arsenic also occurs in an adsorbed phase on metals, mainly adsorbed onto iron. Unlike other metalloids As can be mobilised at pH values found in groundwater both under oxidising and reducing conditions (Smedley and Kinniburgh, 2002). Geogenic As is often related to volcanic deposits and sulfidic minerals such as pyrite.

Arsenic is being used for a wide array of purposes. It is obtained as a by-product of the smelting of lead, cobalt, copper and gold ores. It has been used therapeutically for thousands of years. During the nineteenth century it was very common to treat leukaemia and several skin conditions with a solution of As. Today it is still being used in Chinese medicines but also still as part of a treatment for leukaemia (Ratnaike, 2003; Shen et al, 1997). As also has many industrials uses. Amongst them agricultural applications, wood treatments, pesticides and semiconductors (Brown et al., 2010).

Long-term exposure to high concentrations of As has many adverse effects on the human body. The chemical properties of As are similar to phosphorus, which is critical to many biochemical processes in the body. As substitutes phosphorus in these processes and this has adverse metabolic effects (Manahan, 2002). Consumption of high amounts of arsenic may be through drinking polluted water or eating crops that were irrigated with contaminated water. Although uncommon, acute As poisoning also occurs (Naujokas et al., 2013). Chronic poisoning leads to various medical conditions that include several skin lesions such as hyperpigmentation and hyperkeratosis and eventually cancer. The manifestations are often grouped as arsenicosis (Das, 2008). Both the chemical structure and the oxidation state affect the toxicity and the mobility of arsenic. As(III) is more toxic than As(V) and gets mobilized into groundwater and living cells (Shrivastava et al., 2015).

3.2 Release mechanisms

There are varying mechanisms for the release of arsenic. Amongst these processes are reductive dissolution, alkali desorption, sulphide oxidation and geothermal activity (Ravenscroft, 2009). Small particles may be eroded in the Himalayas and transported by rivers and glaciers. During transport by rivers or glaciers some of the present iron is turned into iron oxide. The iron oxide forms a coating around the particles and adsorbs As from the river water. During sediment burial decaying organic matter breaks down the iron oxyhydroxides (FeOOH). In the process of dissolution of the FeOOH the sorbed arsenic load is released from its solid state. The biodegradation of peat during burial is widely accepted as the driving mechanism for the release of arsenic in the GBM delta (McArthur, 2001). Other

sources or organic matter are not abundant enough or are not reactive enough to cause the required reduction (Ravenscroft, 2001). The concentrations of arsenic in river waters are very little and cause no problems. Adsorbed to iron oxides, the arsenic is stable which causes no health risks.

The water produced by the reductive dissolution is characterised by high concentrations of iron (Fe) and bicarbonate and low concentrations of nitrate and sulphate (Ravenscroft, 2009). McArthur et al. (2004) sampled groundwater at three locations in the North 24 Parganas district in the state of West Bengal, and found high concentrations of As accompanied by high concentrations of Fe. Ghosh et al. (2015) evaluated water samples from three locations in the Nadia district of West Bengal, and found as well corresponding high concentrations of arsenic and iron. McArthur et al. (2004) also found that concentrations of As in groundwater are high when all FeOOH is reduced. Where reduction of FeOOH is incomplete, As is sorbed to residual FeOOH. In Bihar samples from multiple districts adjacent to the Ganges river show high concentrations of As (Saha, 2009).

3.3 Transport mechanisms

The movement of ions in sediment is controlled by mass transport in pore fluid and groundwater. Advection is migration caused by water flow and diffusion is migration caused by concentration differences. Advection, the motion of particles along the bulk flow, is a transport mechanism significantly faster than diffusion, the net movement of particles. However, in media with low porosity, advection is negligible and diffusion is the only way of transport (Apello and Postma, 2005).

The abundant presence of organic matter causes the release of sorbed As from the clay particles to the pore fluid. The As becomes soluble and mobile. Gravity causes compaction of the deposited sediments. This gravitational force rearranges the orientation of plate shaped clay minerals to a 90-degree angle with the stress direction. This process occurs already in the early stages of compaction, at pressures of only a few kg per cm^2 (Maede, 1996). The law of conservation of mass states both water and particles are incompressible. The water in the pores is forced to move and the dissolved As is transported. Advection also occurs due to non-vertical pressure gradients. The cause of these pressure gradients may be anthropogenic, such as well pumping, or naturogenic, such as quartz cementation. The geomorphological setting of the IGP controls the transport mechanisms. The transport of water within and across the morphological features varies throughout the fluvial system. From the low permeable clay plug, part of the water will move to the adjacent point bar that consists of more permeable sands. Thus, in the early stages of compaction, when the porosity of the clay is relatively high, compaction will cause the As to migrate from the clay to the sands by advection.

Compaction reduces the porosity of the clay significantly. Once the porosity of the clay plug is too low for advection, diffusion becomes the dominating transport mechanism. Water in the pores of the point bar sands contain none or very little soluble As and this gradient results in diffusion from the As in the clay's pore water to the sands' pore water. Diffusion is the movement of molecules down their concentration gradient. Fick's first law describes the diffusion process, but some assumptions are done. First, the system must be at steady state; secondly, the medium must be homogeneous. Fick's first law is given by:

$$J = -D\nabla C \qquad \textit{(Equation 3.1)}$$

D is the diffusion coefficient, a material specific property, and *C* is the concentration. With some modifications Fick's first law for transport through a membrane is given by:

$$J = K\Delta \mathrm{C} \qquad \textit{(Equation 3.2)}$$

With J the diffusion flux [mol $m^{-2}s^{-1}$], K the hydraulic conductivity of the medium [m s^{-1}] and ΔC the difference in concentration [mol/m^3]. The permeability of the clay plug is significantly lower than the permeability of the sandstone; therefor the flux will be predominantly controlled by flux through the clay. K in *Equation 3.2* then refers to the hydraulic conductivity of the clay plug and ΔC is the difference on concentration of As in the clay plug and the point bar. This relation is used to estimate the flux of As from the clay plug to the adjacent point bar.

Once the dissolved As reaches the permeable sand of the point bar, advection becomes the controlling transport mechanism again. Pressure gradients caused by well pumping or differences in hydrostatic pressure and differences in permeability result in groundwater flow. Within the point bar, flow will be favourable along the high-permeable base of the point bar. On the high grounds of the point bar, tube wells are installed for groundwater extraction. The pressure gradient by the extraction draws the groundwater up from the base of the point bar. The clay drapes formed during flood periods function as impermeable boundaries compartmentalising the point bar sands. The water contaminated with As moves along these surfaces to the bottom of the tube wells (Donselaar et al., 2016). *Figure 3.1* provides a generic overview of the transport of As in groundwater from the clay plug to and within the adjacent point bar.

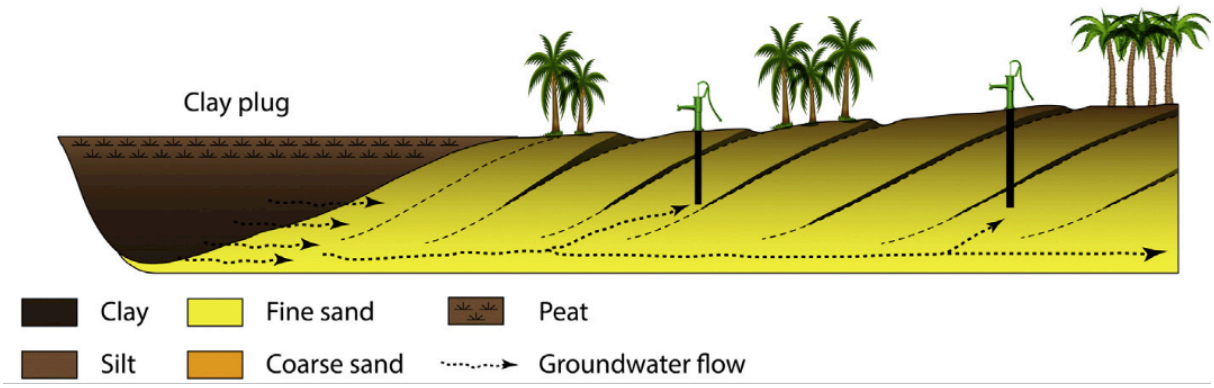

Figure 3.1: Generic model of the transport of As in pore water in geomorphological clay plug and point bar sands. From Donselaar et al. (2016).

Data and Methodology

This section will illustrate the methods used to quantify the potential volume of arsenic available in recent clay plugs in the Holocene Ganges River floodplain. First the data acquisition with Google Earth Pro is described. Second the approach for calculating the volume of the clay plug is thoroughly explained. With these outcomes and data from other studies the potential As volumes are calculated. Finally the approach for estimating migration times is given.

4.1 Data gathering

To gather data of abandoned meander bends, Google Earth Pro was used. This study focussed on the Ganges River and its tributaries throughout the state of Bihar, India. The Ganges River is the dominant river throughout the state. The Gandak River, the Kosi River The Ghaghara River and the Sone River join the Ganges. *Figure 4.1* provides an overview of the main rivers in Bihar and marks the area of this study. Most selected clay plugs are associated with the Ganges River, however some were detected within in the channel belt of the other rivers. The clay plugs vary in size, in general the abandoned meander bends from the Ganges River are larger than the plugs formed by smaller rivers. In Google Earth Pro the built-in tool for constructing paths was used, to mark the outlines of a clay plug. The abandoned meander bend was marked by four line segments, respectively the inner bend, the outer bend and two sides. The outlines were recognised by eye and supported by the built-in tool showing elevation profiles. In total twenty clay plugs were selected. *Figure 4.2* provides an overview of the locations of these clay plugs.

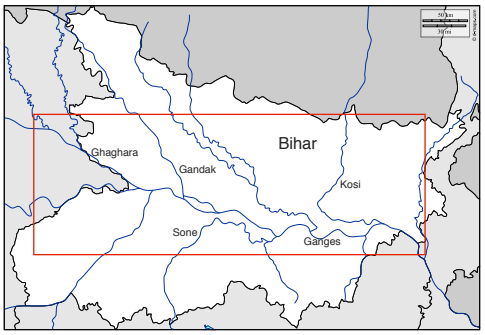

Figure 4.1: Area of studied clay plugs (red) from the Ganges River and its tributaries in the state of Bihar, India.

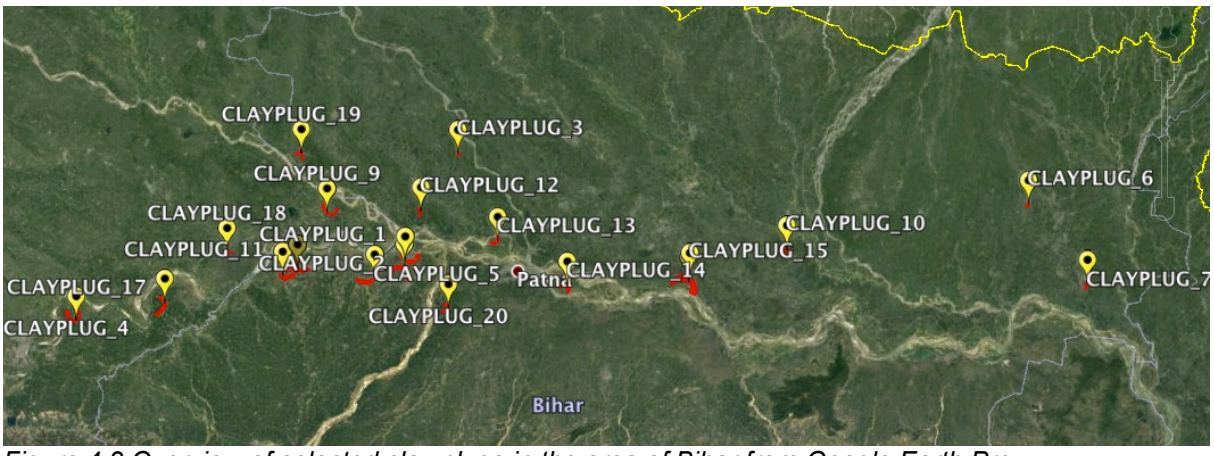

Figure 4.2 Overview of selected clay plugs in the area of Bihar from Google Earth Pro

The collected data of twenty sets of these four line segments was exported to Matlab to create a geometric figure that can be used to approximate the volume of the clay plug. Because it is not possible to use raw data for calculations and simulations, a geometric figure of the clay plugs was needed. The following method describes the process for one clay plug; this was repeated for all twenty plugs.

4.2 Calculating clay plug properties

In Matlab the line segments of the inner and outer bend were best approximated by two different ellipsoids. These best-fit ellipsoids were found using the Gauss-Newton iteration process for non-linear least square problems. The line segments are best approached by using the linear least square method. The data of clay plug one and corresponding fits are shown in Figure 4.3. The plots of the data and the best fits of the other clay plugs can be found in the appendix.

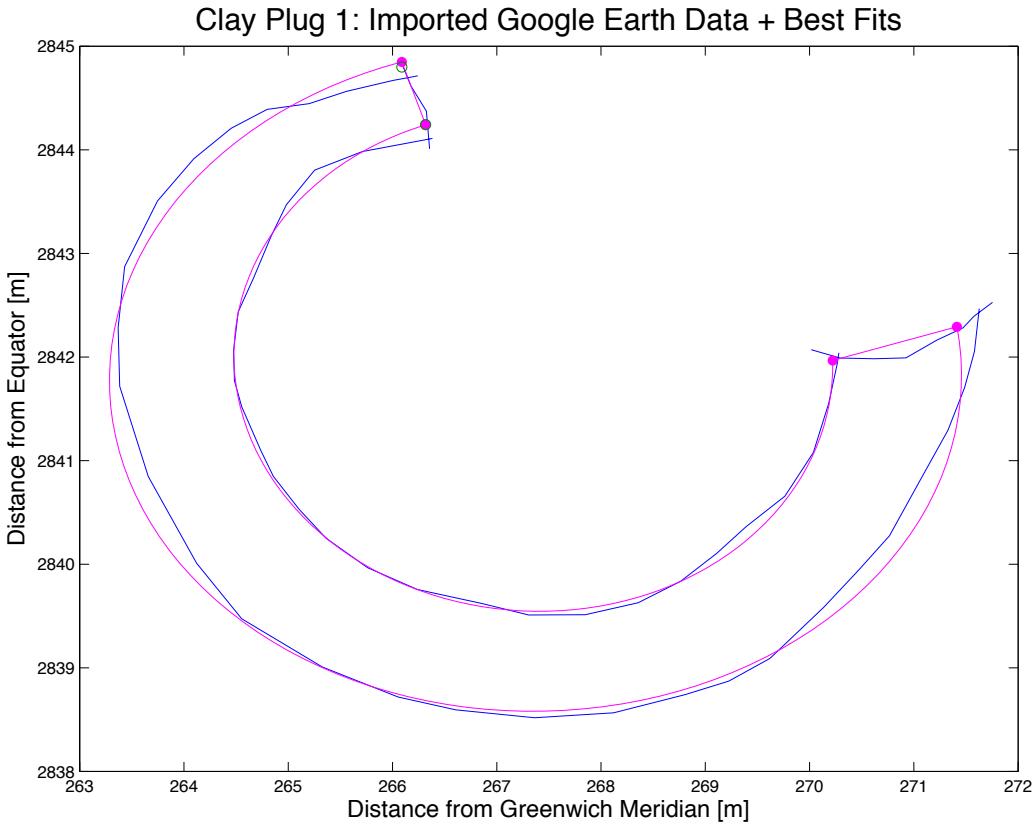

Figure 4.3: Original Google Earth Pro data (blue) and best fitting lines (magenta) of clay plug 1 plotted

To simulate the surface area of the clay plug, the intersections of the two ellipsoids and the two lines were found first. To calculate the simulated surface area, the horseshoe shaped figure was divided into 1000 small pieces. By approximation these pieces are rectangles with constant length and constant width. For each rectangle the length and width were calculated by taking the average of the two sides. The total surface is given by the sum of the area of all these small rectangles. *Table 4.1* presents an overview of the calculated surface areas per clay plug.

Table 4.1: Calculated surface area per clay plug

Surface Area [m^2]			
#		**#**	
1	$1.52 \cdot 10^7$	11	$2.19 \cdot 10^7$
2	$1.15 \cdot 10^7$	12	$2.01 \cdot 10^6$
3	$4.12 \cdot 10^5$	13	$4.62 \cdot 10^6$
4	$8.56 \cdot 10^6$	14	$6.64 \cdot 10^6$
5	$1.51 \cdot 10^7$	15	$1.32 \cdot 10^7$
6	$9.64 \cdot 10^5$	16	$1.69 \cdot 10^7$
7	$1.83 \cdot 10^6$	17	$9.76 \cdot 10^6$
8	$9.76 \cdot 10^6$	18	$4.39 \cdot 10^6$
9	$5.92 \cdot 10^6$	19	$2.72 \cdot 10^6$
10	$3.28 \cdot 10^6$	20	$3.67 \cdot 10^6$

Google Earth Pro also provides a built-in tool for polygons. This tool is used to outline the clay plug again. To check the calculated surface area of the simulation, the outcome is compared to the value given by Google Earth Pro. Two factors have influenced potential differences. Naturally the first is the best-fit method used to approximate the clay plug. Second are manual errors made while using the polygon tool, when overlaying the first set of clay plug borders. The error was calculated as a percentage expressing the difference between the area supplied by Google Earth Pro and the calculated area. The average error was 4.65%.

For the 3D approximation of the volume of the clay plug a depth profile was constructed. To simulate the depth profile a maximum depth was to be determined. Based on core descriptions and interpretations from Donselaar et al. (2016) the thickness of a clay plug is 12 meter. This thickness was used as the maximum depth for the cross sectional profile of the clay plug. The first profile is a generic approach based on a fixed deepest point. The profile consisted of two straight lines that intersected at the maximum depth of 12 m. This depth profile is shown in *Figure 4.4a.* The profile represented a very thin, cross sectional slice of the clay plug. For this thin slice the area was calculated. Helicoidal flow in the meandering river leads to accumulation of sediment up the point bar in the inner bend and erosion of the cut bank in the outer bend (Schumm, 1977). This results in a steep eroded slope in the outer bend and a gentle slope on the inner bend of the meander. *Figure 4.5* shows a top view and cross-sectional overview of helicoidal flow and maximum water velocities in a meandering river (Galloway and Hobday, 1996). To obtain a more realistic depth profile the position of the deepest point with respect to the inner and outer bends was changed. This created an asymmetrical depth profile for the clay plug; the profile is shown in *Figure 4.4b.* Calculations showed that the position of the deepest point with respect to the cut bank and point bar did not affect the area of the slice. Next, the volume of a small rectangle was calculated by multiplying the area of the slice with the width of the rectangle. For calculating the total volume of the clay plug, again the sum of all rectangle-elements was taken.

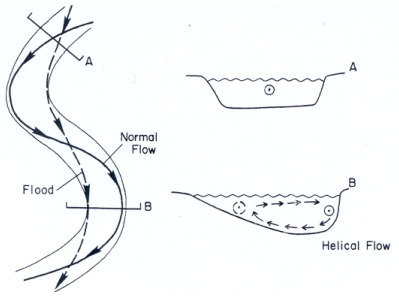

Figure 4.5: Helicoidal flow in a meandering river, top view and cross-sectional profiles from Galloway and Hobday (1996)

As the third approach for the generic depth profile the combination of a parabola and a linear function was used. The profile is shown in *Figure 4.4c*. The model has a fixed deepest point and a fixed position of this deepest point with respect to the edges. To approximate the steep slope of the cut off bank, this position is set at a fraction 1/10 of the width of the clay plug with respect to the outer bend (cut bank). The equations for both the parabola and the linear line were integrated to calculate the area under the functions. Again the total volume was calculated by calculating the volume of a small rectangle and the sum of all these volumes. The volumes of the clay plugs calculated with the varying depth profiles were compared and were of similar magnitude. The third depth profile is a more realistic approach and therefor these calculated volumes are listed in *Table 4.2.*

Table 4.2: Calculated volumes per clay plug

Volume [m^2]			
#		**#**	
1	$9.47 \cdot 10^7$	11	$1.36 \cdot 10^8$
2	$7.14 \cdot 10^7$	12	$1.25 \cdot 10^7$
3	$2.57 \cdot 10^6$	13	$2.87 \cdot 10^7$
4	$5.32 \cdot 10^7$	14	$4.13 \cdot 10^7$
5	$9.41 \cdot 10^7$	15	$8.23 \cdot 10^7$
6	$5.99 \cdot 10^6$	16	$1.05 \cdot 10^8$
7	$1.14 \cdot 10^7$	17	$6.07 \cdot 10^7$
8	$6.07 \cdot 10^7$	18	$2.73 \cdot 10^7$
9	$3.68 \cdot 10^7$	19	$1.69 \cdot 10^7$
10	$2.04 \cdot 10^7$	20	$2.28 \cdot 10^7$

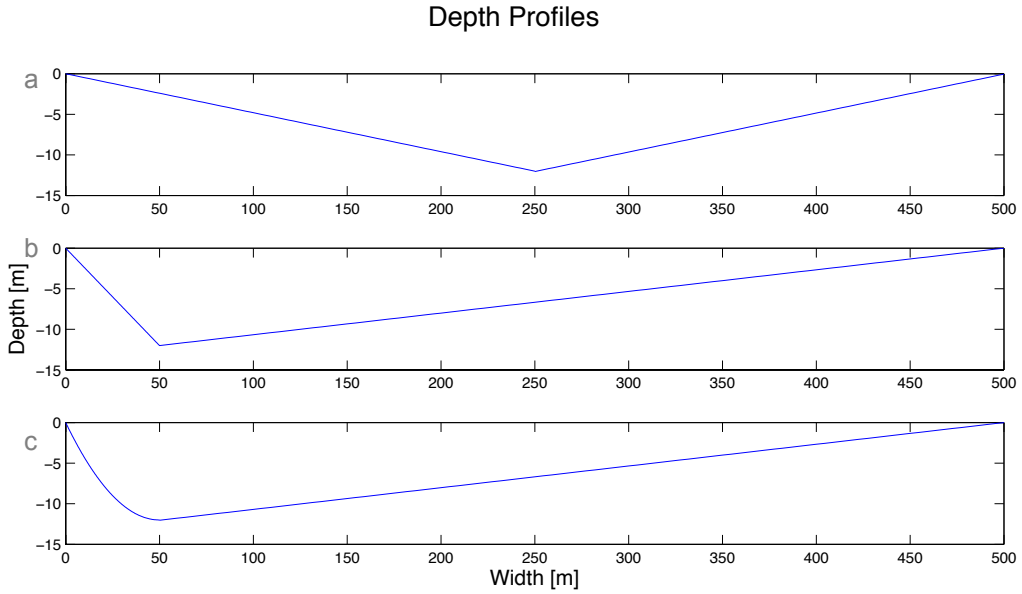

Figure 4.4abc: a. Depth profile 1; two straight lines meeting at fixed depth (12 m) at halfwidth. b: Depth profile 2; two linear lines meeting at fixed depth (12 m) at 1/10th of total width. c: Depth profile 3; linear line and parabola meeting at fixed depth (12 m) at 1/10th of total width.

4.3 Calculating potential arsenic volumes

Well data from Ghosh et al. (2015) shows the upper 12 meter that corresponds to the clay plug does not consist of solely clay. To establish a more specific density this information was taken into account. Data from the Haringhata well and well 204 (Ghosh et al., 2015) were used to calculate an averaged composition of grainsize. Based on porosity values from Freeze and Cherry (1979) coarse sand, fine sand and silt were grouped together since porosities vary little. For the weight of the sand the density of quartz was used. For the weight of the clay the density of multiple clay minerals was used to calculate an average. The minerals used are kaolite, illite and montmorillonite. The porosity of the sediment is also of large influence on the calculated weight of the body. Gravity causes compaction of the deposits. The compaction of sediment is primarily controlled by its mineralogic composition. The resistance to compaction is strongly correlated with the average grain size of the sediment. Clay rich sediments have porosities ranging from 40% up to 95% before compaction (Holbrook, 2001). For clay rich sediments in oxbow lakes initial porosities range from 70% to 90% (Singer and Müller, 1983). The initial porosity of unconsolidated sand varies from 35% to 50% (Stone and Siever, 1996). The sediments are deposited as standing water body sediments and porespace is predominantly filled with water. For these

calculations complete water saturation was assumed. This information was used to account for the water content and its weight as well. The grainsize data from Ghosh et al. (2015) from the Haringhata Well and Well 204 are shown in *Table 4.3ab.* The calculated average grain sizes are shown in *Table 4.4.*

Table 4.3ab: Well data Ghosh et al. (2015), grainsize distribution upper twelve meters of the Haringhata well and well 204

Haringhata Well			
0-6 m		6-12 m	
%	Grainsize	%	Grainsize
14	Coarse sand	10	Coarse sand
32	Fine sand	20	Fine sand
31	Silt	15	Silt
23	Clay	55	Clay

Well 204			
0-6 m		6-12 m	
%	Grainsize	%	Grainsize
1,3	Coarse sand	1	Coarse sand
17,7	Fine sand	8	Fine sand
52	Silt	60	Silt
29	Clay	31	Clay

Table 4.4: Average grainsize distribution based on well data Ghosh et al. (2015) for the upper 12 meter of clay plugs in the area of Bihar

Average Distribution	
0-12 m	
%	Grainsize
6,6	Coarse sand
19,4	Fine sand
39,5	Silt
24,5	Clay

Ghosh et al. (2015) also provided data on As concentrations in their tube wells. Based on this data an average As content in g/kg sediment was calculated. For these calculations there was no differentiation between the upper and lower part of the clay plug because calculations are estimates of the magnitude of the orders and more precise concentrations will not affect these estimates. Ghosh et al. (2015) found on average 21.2 mg As per kg sediment in the upper 6 m and 14.2 mg As per kg sediment from 6 to 12 meter depth. For this research these values were averaged. The average arsenic content in the upper 12 meter used for this research is 17.7 mg As per kg sediment.

For the final estimation of the potential As volume in the clay plugs one last calculation was done. The product of the calculated weight of the clay plug and the As content was taken. Again a minimum and maximum value for these results were provided. *Table 4.5* shows the minimum and maximum volumes of As in kg, in each clay plug.

Table 4.5: Calculated minimum and maximum volume of As per clay plug

Volume As [kg]					
#	Minimum	Maximum	#	Minimum	Maximum
1	$2.77 \cdot 10^6$	$3.34 \cdot 10^6$	11	$3.97 \cdot 10^6$	$4.79 \cdot 10^6$
2	$2.09 \cdot 10^6$	$2.52 \cdot 10^6$	12	$3.65 \cdot 10^5$	$4.40 \cdot 10^5$
3	$0.08 \cdot 10^6$	$0.09 \cdot 10^6$	13	$8.39 \cdot 10^5$	$1.01 \cdot 10^6$
4	$1.55 \cdot 10^6$	$1.87 \cdot 10^6$	14	$1.21 \cdot 10^6$	$1.46 \cdot 10^6$
5	$2.75 \cdot 10^6$	$3.3 \cdot 10^6$	15	$2.41 \cdot 10^6$	$2.90 \cdot 10^6$
6	$1.75 \cdot 10^5$	$2.11 \cdot 10^5$	16	$3.06 \cdot 10^6$	$3.70 \cdot 10^6$
7	$3.32 \cdot 10^5$	$4.01 \cdot 10^5$	17	$1.77 \cdot 10^6$	$2.14 \cdot 10^6$
8	$1.77 \cdot 10^6$	$2.14 \cdot 10^6$	18	$7.98 \cdot 10^5$	$9.63 \cdot 10^5$
9	$1.08 \cdot 10^6$	$1.30 \cdot 10^6$	19	$4.95 \cdot 10^5$	$5.97 \cdot 10^5$
10	$5.96 \cdot 10^5$	$7.19 \cdot 10^5$	20	$6.67 \cdot 10^5$	$8.05 \cdot 10^5$

4.4 Estimating diffusion fluxes

For the estimation of the initial flux from the clay plug to the point bar, first the potential As volumes were used. Next the contact area between the clay plug and the adjacent point bar was calculated. In these calculations the location of the deepest point with respect to the cut bank is crucial. This point was still set at $1/10^{th}$ of the total width of the clay plug. To calculate the total contact area, a similar approach was used to earlier calculations of the total surface

area and total volume. 1000 Small rectangular area elements were created. Per rectangle the average length along the point bar slope and the average width were calculated. For each rectangle-element the contact surface was determined. For calculating the total contact area, the sum of all elements was taken. There are no known driving forces in the point bar for the release of As from its solid state. Therefor, for these calculations is it assumed that the concentration of soluble As in the pore fluid of the point bar sands is negligible. For the hydraulic conductivity crucial to the modified version of Fick's first law the following range was used: a minimal hydraulic conductivity of $1{\cdot}10^{-8}$ m/s and a maximal value of $1 \cdot 10^{-7}$ m/s (Bear, 1972). Because for all clay plugs the same As concentration was used, the initial flux [g/m^2] of arsenic to the point bar is the same for every plug. The discharge [kg/day] however, is based on the initial flux and the contact surface. This property does vary for all clay plugs. A minimum and maximum value were calculated for this discharge. Because the discharge depends linearly on the hydraulic conductivity, this soil property is of large influence over time. The discharge also depends on the present As volume. Over time the volume will decrease and thus the discharge will decrease. The discharge decreases exponentially over time. This relation can be seen in *Figure 4.6*. This figure displays the minimum initial discharge of clay plug 1 combined with the minimal hydraulic conductivity over time. For the other nineteen clay plugs the discharge over time shows a similar exponential decrease.

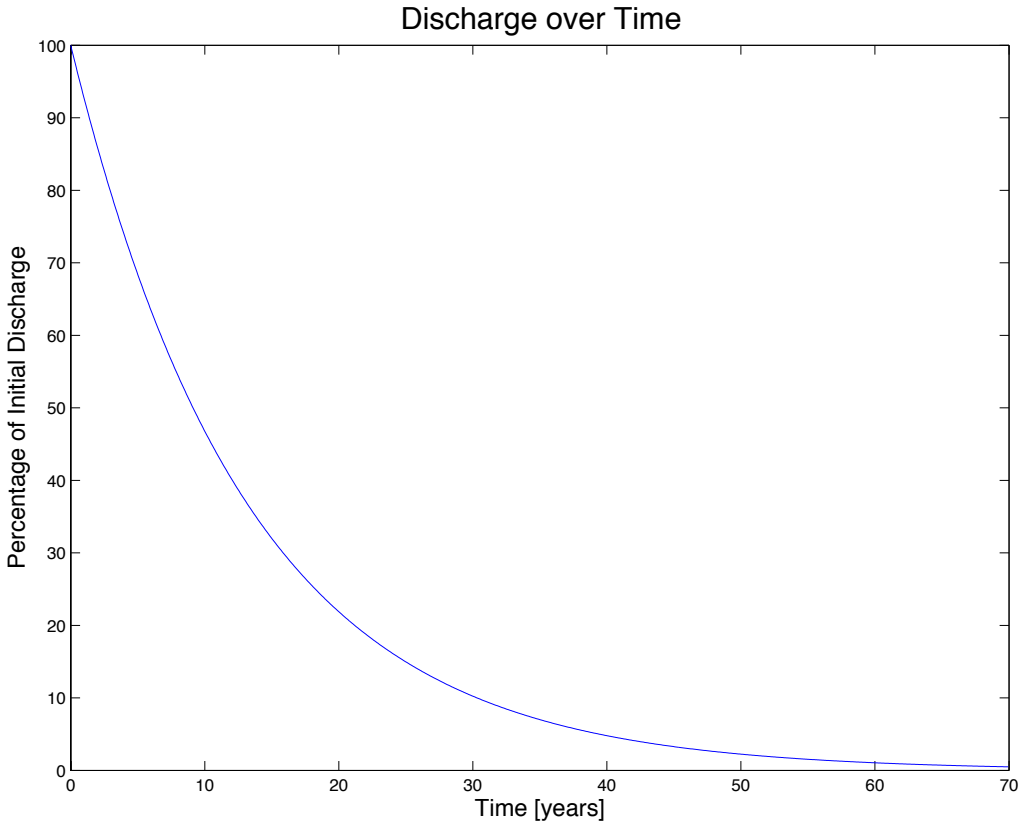

Figure 4.6: Initial discharge over time from clay plug 1 when assuming minimum hydraulic conductivity

All discussed non-varying properties used for calculations are compiled in *Table 4.5.* The script used for all calculations can be found in the appendix. *Table 4.6* provides an overview of all calculated parameters unique per clay plug.

Table 4.5: Clay plug properties

Clay Plug Properties	
Depth [m]	12
Min. Porosity	0.3672
Max. Porosity	0.6029
Min. Density Sediment incl. Water [kg/m^3]	$1.651 \cdot 10^3$
Max. Density Sediment incl. Water [kg/m^3]	$1.992 \cdot 10^3$
Min. Hydraulic Conductivity [m/s]	$1 \cdot 10^{-8}$
Max. Hydraulic Conductivity [m/s]	$1 \cdot 10^{-7}$
Arsenic content [g/kg sediment]	0.0177
Min. Initial Diffusion Flux [g/(m^{2}year)]	15.286
Max. Initial Diffusion Flux [g/(m^{2}year)]	302.705

Table 4.6: Overview of calculated parameters per clay plug

#	Coordinates	Surface Area [m^2]	Contact Area [m^2]	Volume [m^3]	Min. vol. As [kg]	Max. vol. As [kg]	Min. initial discharge [kg/day]	Max. initial discharge [kg/day]
1	25° 39.355'N 84° 39.656'E	$1.52 \cdot 10^7$	$1.37 \cdot 10^7$	$9.47 \cdot 10^7$	$2.77 \cdot 10^6$	$3.34 \cdot 10^6$	574	11375
2	25° 37.613'N 84° 39.456'E	$1.15 \cdot 10^7$	$1.03 \cdot 10^7$	$7.14 \cdot 10^7$	$2.09 \cdot 10^6$	$2.52 \cdot 10^6$	433	8573
3	26° 3.925'N 84° 53.489'E	$4.12 \cdot 10^5$	$3.74 \cdot 10^5$	$2.57 \cdot 10^6$	$0.08 \cdot 10^6$	$0.09 \cdot 10^6$	16	310
4	25° 25.556'N 83° 14.080'E	$8.56 \cdot 10^6$	$7.70 \cdot 10^6$	$5.32 \cdot 10^7$	$1.55 \cdot 10^6$	$1.87 \cdot 10^6$	323	6387
5	25° 35.235'N 84° 31.741'E	$1.51 \cdot 10^7$	$1.36 \cdot 10^7$	$9.41 \cdot 10^7$	$2.75 \cdot 10^6$	$3.3 \cdot 10^6$	571	11297
6	25° 49.739'N 87° 20.673'E	$9.64 \cdot 10^5$	$8.68 \cdot 10^5$	$5.99 \cdot 10^6$	$1.75 \cdot 10^5$	$2.11 \cdot 10^5$	36	720
7	25° 30.835'N 87° 35.498'E	$1.83 \cdot 10^6$	$1.65 \cdot 10^6$	$1.14 \cdot 10^7$	$3.32 \cdot 10^5$	$4.01 \cdot 10^5$	69	1365
8	25° 37.660'N 84° 11.864'E	$9.76 \cdot 10^6$	$8.79 \cdot 10^6$	$6.07 \cdot 10^7$	$1.77 \cdot 10^6$	$2.14 \cdot 10^6$	368	7288
9	25° 50.598'N 84° 19.553'E	$5.92 \cdot 10^6$	$5.33 \cdot 10^6$	$3.68 \cdot 10^7$	$1.08 \cdot 10^6$	$1.30 \cdot 10^6$	223	4422
10	25° 40.652'N 86° 17.754'E	$3.28 \cdot 10^6$	$2.96 \cdot 10^6$	$2.04 \cdot 10^7$	$5.96 \cdot 10^5$	$7.19 \cdot 10^5$	124	2451
11	25° 35.996'N 84° 7.981'E	$2.19 \cdot 10^7$	$1.97 \cdot 10^7$	$1.36 \cdot 10^8$	$3.97 \cdot 10^6$	$4.79 \cdot 10^6$	825	16329
12	25° 50.720'N 84° 43.835'E	$2.01 \cdot 10^6$	$1.81 \cdot 10^6$	$1.25 \cdot 10^7$	$3.65 \cdot 10^5$	$4.40 \cdot 10^5$	76	1499
13	25° 43.683'N 85° 3.485'E	$4.62 \cdot 10^6$	$4.16 \cdot 10^6$	$2.87 \cdot 10^7$	$8.39 \cdot 10^5$	$1.01 \cdot 10^6$	174	3447
14	25° 33.172'N 85° 21.221'E	$6.64 \cdot 10^6$	$5.98 \cdot 10^6$	$4.13 \cdot 10^7$	$1.21 \cdot 10^6$	$1.46 \cdot 10^6$	250	4958
15	25° 34.734'N 85° 52.682'E	$1.32 \cdot 10^7$	$1.19 \cdot 10^7$	$8.23 \cdot 10^7$	$2.41 \cdot 10^6$	$2.90 \cdot 10^6$	499	9888
16	25° 33.731'N 85° 52.338'E	$1.69 \cdot 10^7$	$1.52 \cdot 10^7$	$1.05 \cdot 10^8$	$3.06 \cdot 10^6$	$3.70 \cdot 10^6$	636	12587
17	25° 29.754'N 83° 37.307'E	$9.76 \cdot 10^6$	$8.78 \cdot 10^6$	$6.07 \cdot 10^7$	$1.77 \cdot 10^6$	$2.14 \cdot 10^6$	368	7284
18	25° 41.501'N 83° 53.583'E	$4.39 \cdot 10^6$	$3.95 \cdot 10^6$	$2.73 \cdot 10^7$	$7.98 \cdot 10^5$	$9.63 \cdot 10^5$	166	3279
19	26° 4.375'N 84° 12.969'E	$2.72 \cdot 10^6$	$2.45 \cdot 10^6$	$1.69 \cdot 10^7$	$4.95 \cdot 10^5$	$5.97 \cdot 10^5$	103	2034
20	25° 28.248'N 84° 50.653'E	$3.67 \cdot 10^6$	$3.31 \cdot 10^6$	$2.28 \cdot 10^7$	$6.67 \cdot 10^5$	$8.05 \cdot 10^5$	138	2741

To present a clear overview of the calculated clay plug volumes a histogram was created. From this histogram no statistical properties can be obtained because the number of selected clay plugs is too little. The histogram is shown in *Figure 4.7*

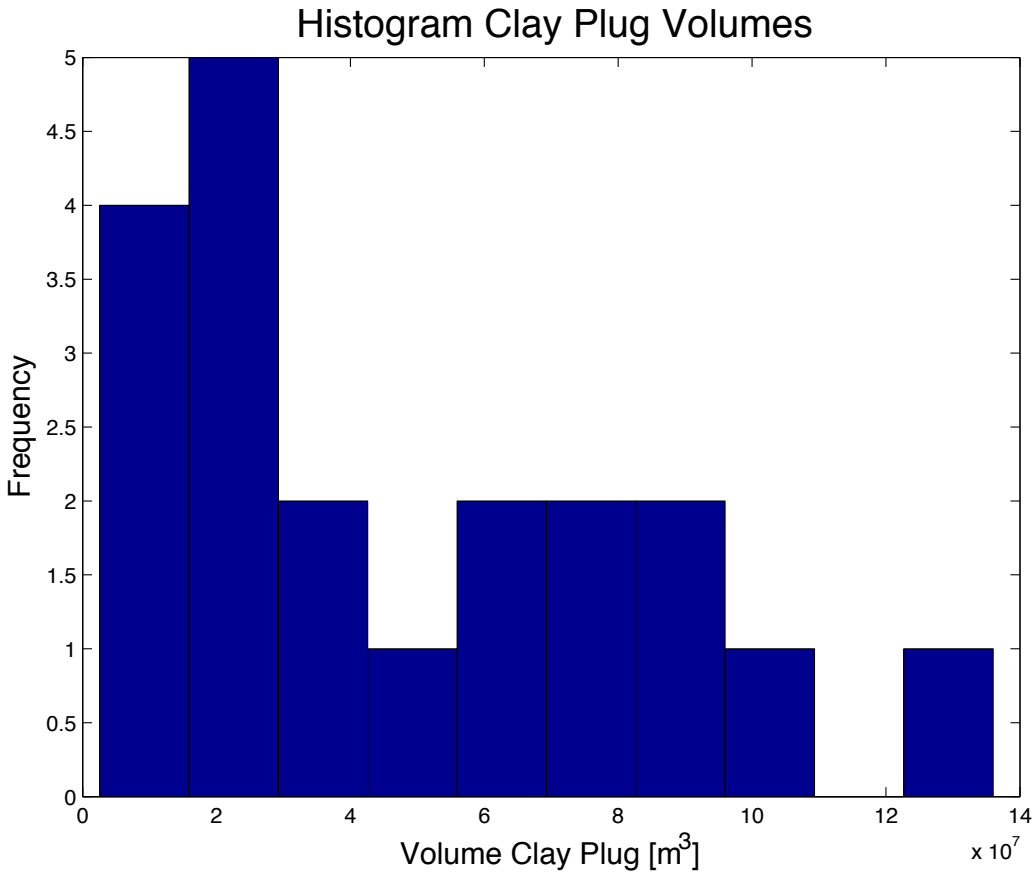

Figure 4.7: Histogram of the calculated potential clay plug volumes

Discussion

The results of this research provide insight on potential As volumes in clay plugs in Holocene Ganges River floodplain deposits. However, the methods used are based on some assumptions and simplifications. When drawing conclusions it is important these are taken into account.

This research was conducted without fieldwork and in-situ sampling. This would minimize uncertainties based on assumptions and estimations. The depth profiles that are used are simplifications of the true depth profile; this adds uncertainties to the model. Measuring depth in recently abandoned clay plugs would improve knowledge of the depth profile. The location of the deepest point is also a simplification of the model, which may be different to the actual situation. The profiles are used for the calculation of the clay plug volume and the contact area between the clay plug and the point bar.

For the calculation of the potential As volume an average grain size distribution was used. This distribution was used for the specific weight of the sediment in the clay plug. This is a simplification and generalisation and for more precision, samples would be needed. Furthermore, the grain size distribution was grouped into two groups, solely differentiating between coarser material (sand and silt) and the finest sediment (clay) based on resembling permeabilities. The two groups are combined with average densities for clay and sand. For clay an average of clay minerals was taken, for sand solely quartz was used. The actual mineralogy of the sediment is unknown and may therefor vary from the values used. For the As content too, an average value based on other studies was used. On site sampling would provide data for better estimations.

The calculations of the flux are just rough estimates because of the assumptions made. The assumption that all As is dissolved, is probably an overestimation. The hydraulic conductivity is linearly related to the diffusion flux. Therefor it is very important to have realistic values for this property. The range of hydraulic conductivities used for this research is general values for fine, unconsolidated, clayey sediment; and true values may differ significantly. The outcomes of the initial flux calculations in this research are therefor rough estimates.

Conclusion

This research shows that clay plugs in Holocene Ganges River floodplain deposits can contain large amounts of As. Under reducing conditions the As is released from its solid state by microbial respiration. Once the As is released to the groundwater, it can migrate to the adjacent point bar by advection and diffusion. Twenty clay plugs were selected in Google Earth Pro and their volumes were simulated based on a depth profile. The outcomes of these calculations were combined with data from previous studies to provide inside on the diffusion flux from the clay plug to the adjacent point bar.

For the simulation of the clay plug bodies, different depth profiles were used. The first consisted of two straight lines meeting halfway at a depth of 12 meter, the thickness of clay plugs based on previous studies. The second profile was a more realistic approach of the cross section of the clay plug. The deepest point was set at 12 meter again but the location was off centred in order to approach the asymmetrical profile of the abandoned meander bend. The third profile consisted again of an off centred maximum depth, but a parabola instead of a linear function now approached the steep cut bank.

The varying depth profiles returned similar volumes for the clay plugs and thus it can be concluded that this profile is not of big influence on the volume calculations. However, for the calculations of the surface area the depth profile and especially the location of the deepest point are of major influence. Since this surface area is used for the calculation of the diffusion flux, it is also of importance for these outcomes to gather data on the depth profile.

From the outcomes of the calculations of the volume of the twenty clay plugs can be concluded that all volumes are in the order of magnitude of 10^6 to 10^8 m^3. However, it is only two larger clay plugs in the order of magnitude of 10^8 and two smaller plug with order 10^6. The two larger clay plugs are abandoned meander bends from the Ganges River, the smaller plugs originated from smaller rivers. For the As volumes a range of outcomes per plug is calculated, these values are all in the order of magnitude of 10^5 to 10^6 kg.

Transport from the dissolved As from the clay plug to the point bar is by advection and diffusion. Gravitational compaction drives pore fluid from the clay sediment into the more permeable point bar sands. Due to concentration differences of As in both morphological features, diffusion also occurs. Based on Fick's First Law the initial diffusion flux was calculated and ranges approximately between 15-300 g/(m^2year). This diffusion flux depends linearly on the hydraulic conductivity. A wide range of values for this property was used and therefor the result is a large range. Diffusion is a very slow process, while advection is reasonably fast. When permeabilities and thus fluid flow are low, it is possible for diffusion to be the controlling factor.

Recommendations

This research provides an indication of potential As volumes in recent clay plugs in Holocene aquifers in Bihar and the Ganges River floodplains. It can contribute to more extensive research. For further studies the recommendations are given below.

First of all this research is based on twenty clay plugs only. To obtain a more solid dataset, it will be necessary to locate a lot more clay plugs. Data of these extra clay plugs can be processed with the model used for this research. The histograms will then provide a more funded overview.

To gain more knowledge on the true depth profile of a clay plug, different on-site methods could be used in recently abandoned meander bends. For the model used in this research, information of location of the deepest point with respect to the cut bank would improve the accuracy. An old-fashioned way to gather depth data would be the use of a mass on a line while sampling depths on a small boat. Perhaps seismic offers a more accurate and modern method of measurement.

In-situ sampling of clay plug sediments could provide insight in the actual grain size distribution, the water content and the mineralogical composition. This data could result in a more accurate density of the sediment and thus a better indication of the clay plug volume. Measurement of As concentrations in the upper 12 – 15 meters of Holocene clay plug sediments would assist in gaining more knowledge on the upper spatial variations of the contamination and would improve the calculations done to obtain the potential arsenic volume. Testing the hydraulic conductivity of the sediment would highly improve the estimations of the diffusion flux.

The calculations for the initial flux are based on a situation without advection. To obtain a more realistic model, research has to be done into interactions and relations of the two transport mechanisms within the present geomorphological settings. The calculated values of initial diffusion flux are rough estimates; this simplified method could be improved to obtain more accurate rates. With more research it would be possible to present ideas on whether the diffusion process significantly contributes to the total transport rate.

References

Apello, C.A.J., Postma, D., 2005. Geochemistry, groundwater and pollution. CRC Press, Boca Raton, USA.

Bear, J., 1972. Dynamics of fluids in porous media. Elsevier, New York, USA.

Berg M., Tran H.C., Nguyen T.C., Pham H.V., Schertenleib R., Giger W., 2001. Arsenic contamination of groundwater and drinking water in Vietnam: A human health threat. Env. Science and Technology, 35, 2621-2626.

BGS, DPHE, 2001. Arsenic contamination of ground water in Bangladesh. In: Kinniburgh, D.G., Smedley, P.L. (Eds.), British Geological Survey Report WC/00/ 19, Final Report, vol. 2, British Geological Survey, Keyworth, UK.

Bhattacharya, P., Chatterjee, D., Jacks, G., 1997. Occurrence of arsenic contaminated groundwater in alluvial aquifers from delta plains, eastern India: options for safe drinking water supply. J. Water Resour. Dev. 13, 79–92.

Brown, R.A., Patterson, K.E., Zimmerman, M.D., Ririe, G.T., 2010. Attenuation of naturally occurring arsenic at petroleum hydrocarbon–impacted sites. In: Fields, K.A., Wickramanayake, G.B. (Eds.) Remediation of chlorinated and recalcitrant compounds. Seventh international conference on remediation of chlorinated and recalcitrant compounds.

Chakraborti, D., Mukherjee, S.C., Pati, S., Sengupta, M.K., Rahman, M.M., Chowdhury, U.K., Lodh, D., Chanda, C.R., Chakraborti, A.K., Basu, G.K., 2003. Arsenic groundwater contamination in Middle Ganges Plain, Bihar, India: a future danger? Environ Health Perspect. 111, 1194–1201.

Chakraborti, D., Rahman, M.M., Ahamed, S., Dutta, R.N., Pati, S., Mukherjee, S.C., 2016. Arsenic groundwater contamination and its health effects in Patna district (capital of Bihar) in the middle Ganges plain, India. Chemosphere 152, 520-529

Das, N.K., Sungupta, S.R., 2008. Arsenicosis: diagnosis and treatment. Indian J Dermatol Venereol Leprol, 74, 571-81.

DeCelles, P.G. & Giles, K.A. 1996. Foreland basin systems. Basin Research, 8, 105-123.

Donselaar, M.E., Bhatt, A.G., Ashok, K., 2016. On the relation between fluvio-deltaic flood basin geomorphology and the wide-spread occurrence of arsenic pollution in shallow aquifers. Science of the Total Environment 574, 901–913.

Freeze, R.A., Cherry, J.A., 1979. Groundwater. Prentice-Hall.

Galloway, W.E., Hobday, D.K., Terrigenous Clastic Depostional Systems. Springer Berlin Heidelberg.

Ghosh, A.K, Singh, S.K., Bose, N., Chaudhary, S., 2007. Arsenic contaminated aquifers: a study of the Ganges levee zones in Bihar, India. Annual Conference 2007, Royal Geographical Society, London

Ghosh, D., Routh, J., Bhadury, P., 2015. Characterization and microbial utilization of dissolved lipid organic fraction in arsenic impacted aquifers (India). J. Hydrol. 527, 221–233.

Ghosh, D., Routh, J., Dario, M., Bhadury, P., 2015. Elemental and biomarker characteristics in a Pleistocene aquifer vulnerable to arsenic contamination in the Bengal Delta Plain, India. Appl. Geochem. 61, 87–98.

Holbrook, P., 2002. The primary controls over sediment compaction. In: Huffman, A.R., Bowers, G.L. (Eds.), Pressure regimes in sedimentary basins and their prediction. AAPG Memoir 76, 21-32.

Kossoff, D, Hudson-Edwards, K.A. 2012. Arsenic in the environment. Chapter 1 in: Santini, M., Ward, S.M. (Eds.), The metabolism of arsenite. Arsenic in the environment series, 5, CRC Press, London, UK, pp. 1-23.

Nath, B., Berner, Z., Mallik, S.B., Chatterjee, D., Charlet, L., Stueben, D., 2005. Characteriza- tion of aquifers conducting groundwaters with high and low arsenic concentrations: a comparative case study from West Bengal, India. Mineral. Mag. 69, 841–854.

Nichols, G., 2009. Sedimentology and stratigraphy. Wiley-Blackwell, Oxford, UK.

Norman, N.C., 1998. Chemistry of arsenic, antimony and bismuth. Thomson Science, London, UK

Meade, R.H., 1966. Factors influencing the early stages of the compaction of clays and sands — review. J. Sediment. Petrol. 36, 1085–1101.

Manahan, S.E., 2003. Toxicological chemistry and biochemistry. CRC Press, Boca Raton, USA.
McArthur, J.M., Ravenscroft, P., Safiullah, S., Thirlwall, M.F., 2001. Arsenic in groundwater: testing pollution mechanisms for sedimentary aquifers in Bangladesh. Water Resour. Res. 37, 109–117.

McArthur, J.M., Banerjee, D.M., Hudson-Edwards, K.A., Mishrab, R., Purohit, R., Ravenscroft, P., Cronine, A., Howarth, R.J., Chatterjee, A., Talukder, T., Lowry, D., Houghton, S., Chadha, D.K., 2004. Natural organic matter in sedimentary basins and its relation to arsenic in anoxic ground water: the example of West Bengal and its worldwide implications. Appl. Geochem. 19, 1255–1293.

Naujokas, M.F., Anderson, B., Ahsan, H., Aposhian, V., Graziano, J.H., Thompson, C., Suk, W.A., 2013. The broad scope of health effects from chronic arsenic exposure: update on a worldwide public health problem. Environ Health Perspect 121, 295–302.

Powers, P.M., Lillie, R.J., Yeats, R.S., 1998. Structure and shortening of the Kangra and Dehra Dun reentrants, Sub-Himalay, India. GSA Bulletin 110, 1010-1027.

Ratnaike, R.N., 2003. Acute and chronic arsenic toxicity. Postgrad Med J 79, 391–396.

Ravenscroft, P., McArthur, J.M., Hoque, B.A., 2001. Geochemical and paleohydrological controls on pollution of groundwater by arsenic. In: Chappell, W.R., Abernathy, C.O., Calderon, R.L. (Eds.), Arsenic Exposure and Health Effects IV. Elsevier, Oxford, UK.

Ravenscroft P., 2007. Predicting the global extent of arsenic pollution of groundwater and its potential impact on human health. Report for UNICEF, New York, USA.

Ravenscroft, P., Brammer, H., Richards, K., 2009. Arsenic in Asia. In: Ravenscroft, P., Brammer, H., Richards, K. (Eds.), Arsenic Contamination: A Global Synthesis. Wiley- Blackwell, Oxford, UK.

Saha, D., 2009. Arsenic groundwater contamination in parts of middle Ganges plain, Bihar. Curr. Science 97.

Shen, Z.X., Chen, G.Q., Ni, J.H., Li, X.S., Xiong, S.M., Qiu, Q.Y., Zhu, J., Tang, W., Sun, G.L., Yang, K.Q, Chen, Y. Zhou, L., Fang, Z.W., Wang, Y.T., Ma, J., Zhang, P., Zhang, T.D., Chen, S.J., Chen, Z., Wang, Z.Y., Use of Arsenic Trioxide (As2O3) in the Treatment of Acute Promyelocytic Leukemia (APL): II. Clinical Efficacy and Pharmacokinetics in Relapsed Patients**.** Blood 89, 3354-3360.

Schumm, S.A., 1977. The Fluvial System. Wiley, New York, USA.

Shrivastava, A., Ghosh, D., Dash, A., Bose, S., 2015. Arsenic contamination in soil and sediment in India: sources, effects, and remediation. Curr. Pollut. Rep. 1, 35–46.

Singer, A., Müller, G., 1983. Diagenesis in argillaceous sediments. In: Larsen, G., Chillingar, G.V. (Eds.), Diagenesis in Sediments and Sedimentary Rocks 2. Elsevier Amsterdam, 115–212.

Singh, I.B., 1996. Geological evolution of the Ganges Plain – an overview. Journal of the Paleontological Society of India 41, 99-137.

Sinha, R, Friend, P.F. 1994. River systems and their sediment flux, Indo-Gangetic plains, northern Bihar, India. Sedimentology, 41, 825-45.

Sinha, R., Tandon, S.K., Gibling, M.R., Bhattacharjee, P.S., Dasgupta, A.S., 2005. Late Quaternary geology and alluvial stratigraphy of the Ganges basin. Himalayan Geology 26, 223-240.

Smedley, P.L., Kinniburgh, D.G., 2002. A review of the source, behavior and distribution of arsenic in natural waters. Appl. Geochem. 17, 517–568.

Smith, A., Goycolea, M., Haque, R., Biggs, M., 1998. Marked increase in bladder and lung cancer mortality in a region of Northern Chile due to arsenic in drinking water. Am. J. Epidemiol. 147, 660–669.

Smith, A.H., Lingas, E.O., Rahman, M., 2000. Contamination of drinking water by arsenic in Bangladesh: a public health emergency. Bulletin World Health Organization 78, 1093–1103.

Stone, W.N., Siever, R., 1996. Quantifying compaction, pressure solution and quartz cementation in moderately- and deeply-buried quartzose sandstones from the Greater Green River Basin, Wyoming. In: Crossey, L.J., Totten, M.W., Scholle, P.A. (Eds.), Siliciclastic Diagenesis and Fluid Flow: Concepts and Applications. SEPM Spec Publ 55 129–150.

Uddin, R., Huda, R.N., 2011. Arsenic poisoning in Bangladesh. Oman Med. J. 26, 207.

World Health Organization, 1993. Guidelines for Drinking-Water Quality. 2nd ed. Recommendations vol. 1.

World Health Organization, 2011. Guidelines for Drinking-Water Quality. 4th ed. Geneva, Switzerland.

Appendix

9.1 Clay plug plots 2-20

Overview clay plug data from Google Earth Pro (blue) and corresponding best fits (magenta).

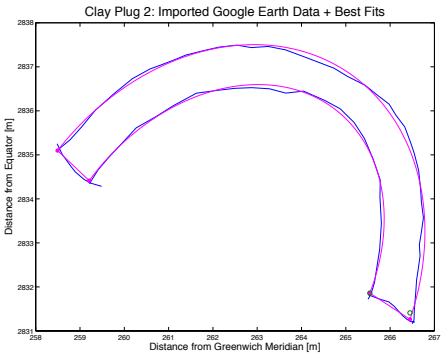

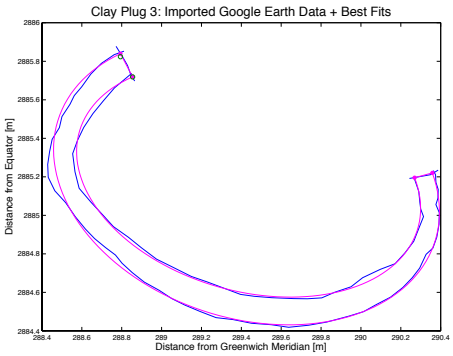

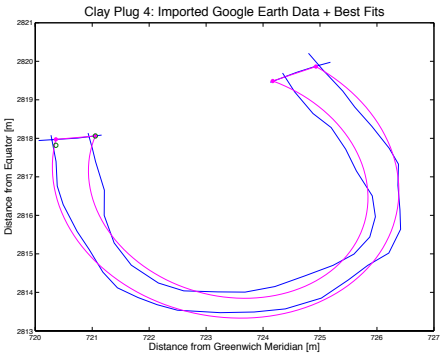

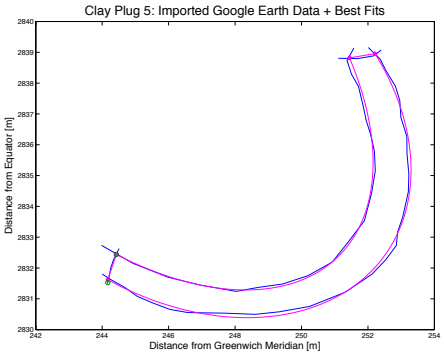

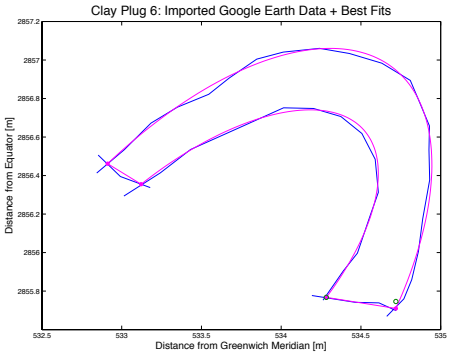

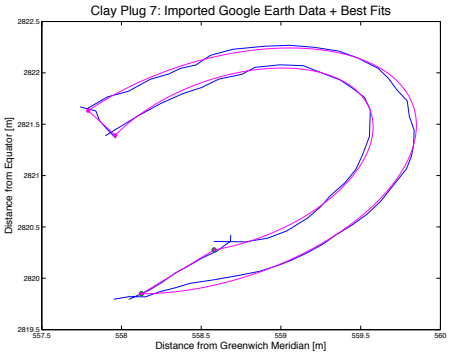

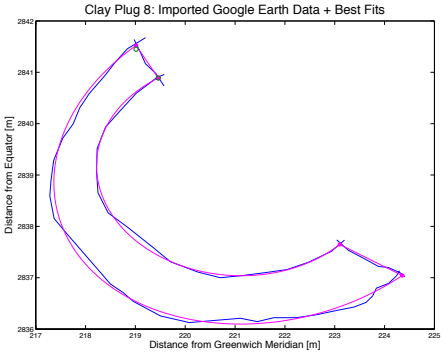

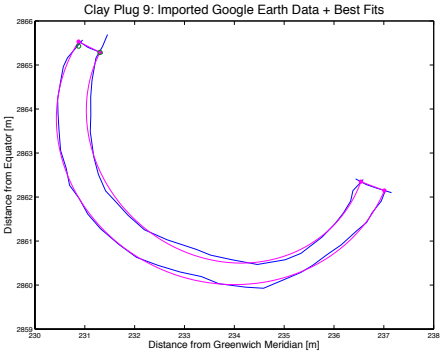

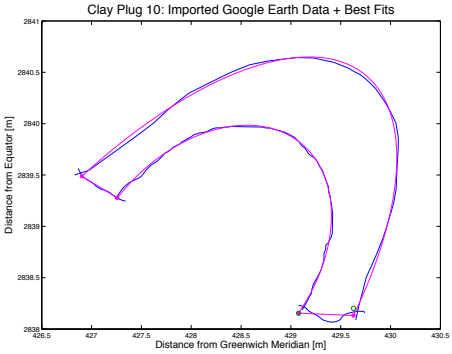

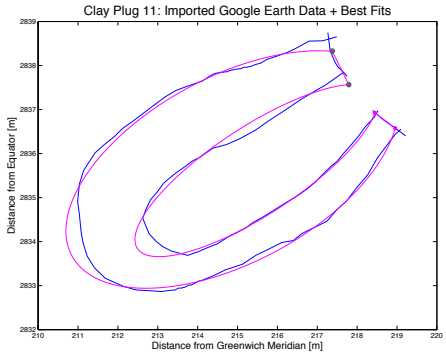
Clay Plug 11: Imported Google Earth Data + Best Fits
Distance from Equator [m]
Distance from Greenwich Meridian [m]

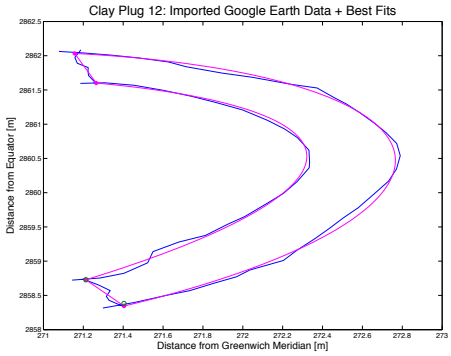
Clay Plug 12: Imported Google Earth Data + Best Fits
Distance from Equator [m]
Distance from Greenwich Meridian [m]

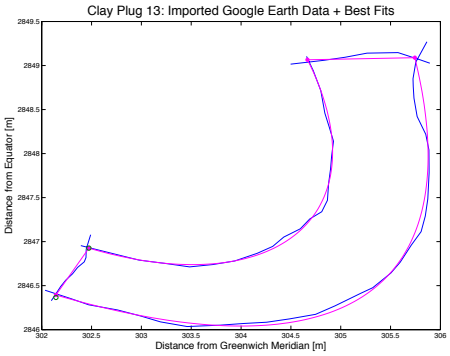
Clay Plug 13: Imported Google Earth Data + Best Fits
Distance from Equator [m]
Distance from Greenwich Meridian [m]

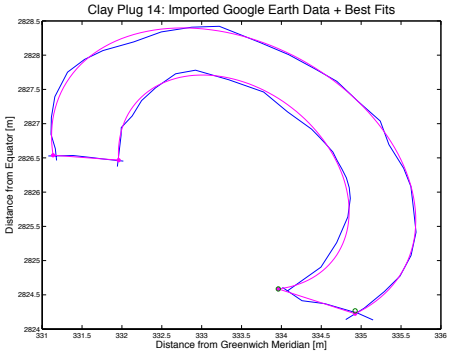
Clay Plug 14: Imported Google Earth Data + Best Fits
Distance from Equator [m]
Distance from Greenwich Meridian [m]

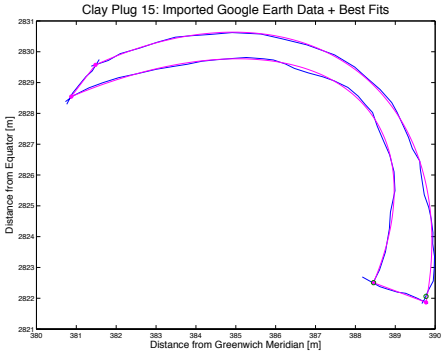
Clay Plug 15: Imported Google Earth Data + Best Fits
Distance from Equator [m]
Distance from Greenwich Meridian [m]

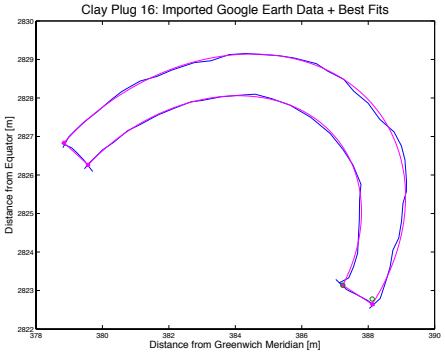
Clay Plug 16: Imported Google Earth Data + Best Fits
Distance from Equator [m]
Distance from Greenwich Meridian [m]

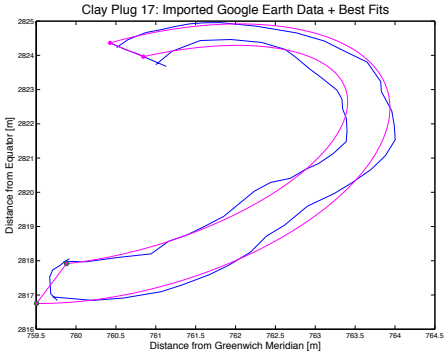
Clay Plug 17: Imported Google Earth Data + Best Fits
Distance from Equator [m]
Distance from Greenwich Meridian [m]

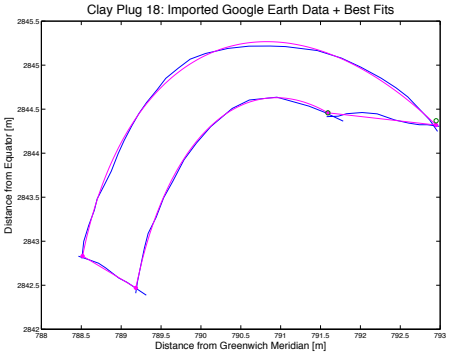
Clay Plug 18: Imported Google Earth Data + Best Fits
Distance from Equator [m]
Distance from Greenwich Meridian [m]

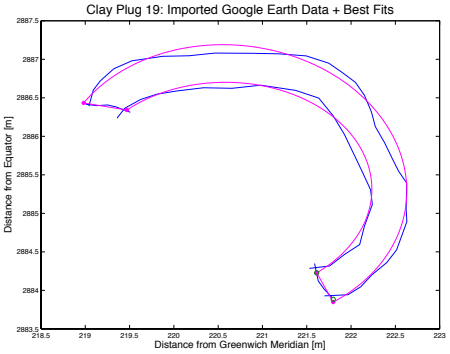
Clay Plug 19: Imported Google Earth Data + Best Fits
Distance from Equator [m]
Distance from Greenwich Meridian [m]

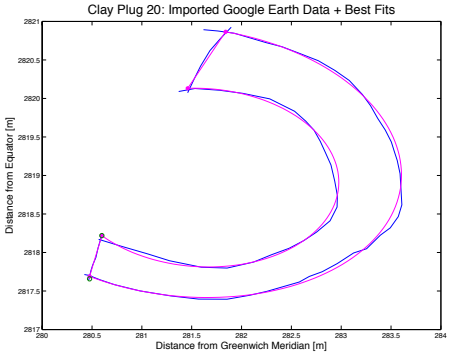
Clay Plug 20: Imported Google Earth Data + Best Fits
Distance from Equator [m]
Distance from Greenwich Meridian [m]

9.1 Matlab Script

Contents


```
% Data folder to path
addpath('/Users/Floortje/Documents/TU Delft/BEP/Data')

clear all
close all
clc
```

Constants

```
Plugs = 1:20; % number of clay plugs
Depth = 12; % maximum depth clay plug[m]
Fraction_W = 1/10; % fraction of width clay plug

Fraction_Diss = 1; % fraction of As dissolved
HC_Min = 1*10^(-8); % Min. hydraulic conductivity clay [m/s] (J. Bear 1973)
HC_Max = 1*10^(-7); % Max. hydraulic conductivity  clay [m/s]
```

Different depth profiles

```
% Plot 3 depth profiles

Width = 500; % Width oxbow [m]
P1_x_DP = Width*0.5; % Location deepest point; exact middle
P2_x_DP = Width*Fraction_W; % Location deepest point;
P3_x_DP = Width*Fraction_W; % Location deepest point;

% Profile 1: Two straight lines, deepest point in the middle
P1_x_1 = linspace(0,P1_x_DP,100);
P1_x_2 = linspace(P1_x_DP,Width,100);
P1_y_1 = (-24/Width)*P1_x_1;
P1_y_2 = (24/Width)*(P1_x_2-P1_x_DP)+(12/(-1/2*Width))-12;
```

```
% Profile 2: Two straigh lines, deepest point off centered
P2_x_1 = linspace(0,P2_x_DP,100);
P2_x_2 = linspace(P2_x_DP,Width,100);
P2_y_1 = ((Depth)/(-P2_x_DP))*P2_x_1+(-Depth-((Depth)/(-P2_x_DP))*P2_x_DP);
P2_y_2 = ((Depth)/(Width-P2_x_DP))*P2_x_2 + ...
         (-Depth-((Depth)/(Width-P2_x_DP))*P2_x_DP);

% Profile 3: Parabolic + straight line, deepest point off centered
P3_P = ((P3_x_DP^2)/(4*Depth))-((P3_x_DP^2)/(2*Depth));
P3_Q = Width-P3_x_DP;
P3_D = P3_Q^2-4*P3_P*-Depth;
P3_C = (-P3_Q + sqrt(P3_D))/(2*P3_P);
P3_x_1 = linspace(0,P3_x_DP,100);
P3_x_2 = linspace(P3_x_DP,Width,100);
P3_y_1 = (Depth/(P3_x_DP^2)).*(P3_x_1-P3_x_DP).^2-Depth;
P3_y_2 = P3_C.*P3_x_2-P3_C*Width;


figure
subplot(3,1,1)
plot(P1_x_1, P1_y_1);
hold on
plot(P1_x_2, P1_y_2);

subplot(3,1,2)
plot(P2_x_1, P2_y_1);
hold on
plot(P2_x_2, P2_y_2);
ylabel('Depth [m]', 'Fontsize', 14)

subplot(3,1,3)
plot(P3_x_1, P3_y_1);
hold on
plot(P3_x_2, P3_y_2);

suptitle('Depth Profiles')

xlabel('Width [m]', 'Fontsize', 14)
```

Prelocating

```
N = numel(Plugs);

Plug_SurfaceArea=zeros(1,N);
Plug_Volume_P1=zeros(1,N);
Plug_Volume_P3=zeros(1,N);
```

```
Plug_ContactArea=zeros(1,N);
Plug_Weight=zeros(2,N);
Plug_As=zeros(2,N);
Plug_Flux=zeros(2,N);
Plug_Q=zeros(2,N);
AS_Conc=zeros(2,N);
W_Vol=zeros(2,N);



for i=1:N

    j=Plugs(i);
close all
clc

% Filename construction
    title_segment1=sprintf('%d_1_Segment.kml',j);
    title_segment2=sprintf('%d_2_Segment.kml',j);
    title_segment3=sprintf('%d_3_Segment.kml',j);
    title_segment4=sprintf('%d_4_Segment.kml',j);

    title_pin=sprintf('CLAYPLUG_%d.kml',j);
```

Loading, converting and plotting Google Earth Pro data

```
% Load kml data
S1_data = kml2struct(title_segment1); % Inner Bend
S2_data = kml2struct(title_segment2); % Outer Bend
S3_data = kml2struct(title_segment3); % Side 1
S4_data = kml2struct(title_segment4); % Side 2
Pin = kml2struct(title_pin); % Pinpoint location clayplug

% Convert Lat & Lon to UTM
[S1_x_data, S1_y_data]=deg2utm(S1_data.Lat,S1_data.Lon);
[S2_x_data, S2_y_data]=deg2utm(S2_data.Lat,S2_data.Lon);
[S3_x_data, S3_y_data]=deg2utm(S3_data.Lat,S3_data.Lon);
[S4_x_data, S4_y_data]=deg2utm(S4_data.Lat,S4_data.Lon);

% Plot data (shows the imported data in x & y coordinates)
figure
plot(S1_x_data/1000,S1_y_data/1000)
hold on
plot(S2_x_data/1000,S2_y_data/1000)
plot(S3_x_data/1000,S3_y_data/1000)
plot(S4_x_data/1000,S4_y_data/1000)
```

```
xlabel('Distance from Greenwich Meridian [m]', 'Fontsize', 14)
ylabel('Distance from Equator [m]', 'Fontsize', 14)
title(sprintf('Clay Plug %d: Imported Google Earth Data',Plugs(i)),...
      'Fontsize',18)
```

Creating Fits and finding intersections

```
% Create fit for ellipsoids (Segments 1&2)
% a = long axis, b = short axis, phi = rotation angle, X0&Y0 = centre coord
[S1_a,S1_b,S1_phi,S1_X0,S1_Y0] = fit_ellipse2(S1_x_data,S1_y_data);
[S2_a,S2_b,S2_phi,S2_X0,S2_Y0] = fit_ellipse2(S2_x_data,S2_y_data);

% Create linear fits (Segments 3&4)
S3_c = polyfit(S3_x_data,S3_y_data,1);
S4_c = polyfit(S4_x_data,S4_y_data,1);

% Find intersections elllipses S1 & S2 with sides S3 & S4
% intersections S1 & S3
[I13_x(1) I13_x(2) I13_y(1) I13_y(2) I13_theta(1) I13_theta(2)] = ...
IntersectEllipseLine(S1_a, S1_b, S1_phi, S1_X0, S1_Y0, S3_c(1), S3_c(2));

% intersections S1 & S4
[I14_x(1) I14_x(2) I14_y(1) I14_y(2) I14_theta(1) I14_theta(2)] = ...
IntersectEllipseLine(S1_a, S1_b, S1_phi, S1_X0, S1_Y0, S4_c(1), S4_c(2));

% intersections S2 & S3
[I23_x(1) I23_x(2) I23_y(1) I23_y(2) I23_theta(1) I23_theta(2)] = ...
IntersectEllipseLine(S2_a, S2_b, S2_phi, S2_X0, S2_Y0, S3_c(1), S3_c(2));

% intersections S2 & S4
[I24_x(1) I24_x(2) I24_y(1) I24_y(2) I24_theta(1) I24_theta(2)] = ...
IntersectEllipseLine(S2_a, S2_b, S2_phi, S2_X0, S2_Y0, S4_c(1), S4_c(2));

% Select intersections
[value idx_13]=min(abs(I13_x-S3_x_data(1)));
I13_x=I13_x(idx_13); I13_y=I13_y(idx_13); I13_theta=I13_theta(idx_13);
[value idx_14]=min(abs(I14_x- S4_x_data(1)));
I14_x=I14_x(idx_14); I14_y=I14_y(idx_14); I14_theta=I14_theta(idx_14);
[value idx_23]=min(abs(I23_x-S3_x_data(1)));
I23_x=I23_x(idx_13); I23_y=I23_y(idx_23); I23_theta=I23_theta(idx_23);
[value idx_24]=min(abs(I24_x-S4_x_data(1)));
I24_x=I24_x(idx_24); I24_y=I24_y(idx_24); I24_theta=I24_theta(idx_24);

% Select relevant part of the ellipse using the equation
F1_theta = sort([I13_theta I14_theta]);
F2_theta = sort([I23_theta I24_theta]);
```

```
% Differentiate Large part & Small part
if abs(diff(F1_theta)) < pi
   F1_theta_L=[F1_theta(1)+2*pi F1_theta(2)];
   F1_theta_S=[F1_theta(1) F1_theta(2)];
else
   F1_theta_L=[F1_theta(1) F1_theta(2)];
   F1_theta_S=[F1_theta(1)+2*pi F1_theta(2)];
end
if abs(diff(F2_theta))< pi
   F2_theta_L=[F2_theta(1)+2*pi F2_theta(2)];
   F2_theta_S=[F2_theta(1) F2_theta(2)];
else
   F2_theta_L=[F2_theta(1) F2_theta(2)];
   F2_theta_S=[F2_theta(1)+2*pi F2_theta(2)];
end
F1_theta_L=sort(F1_theta_L);
F2_theta_L=sort(F2_theta_L);
F1_theta_S=sort(F1_theta_S);
F2_theta_S=sort(F2_theta_S);
% Contruct ellipsoid fits
F1_theta_L_array=linspace(F1_theta_L(1),F1_theta_L(2),100);
F2_theta_L_array=linspace(F2_theta_L(1),F2_theta_L(2),100);
F1_theta_S_array=linspace(F1_theta_S(1),F1_theta_S(2),100);
F2_theta_S_array=linspace(F2_theta_S(1),F2_theta_S(2),100);

F1_x_L=S1_X0+S1_a*cos(F1_theta_L_array)*cos(S1_phi) + ...
            S1_b*sin(F1_theta_L_array)*-sin(S1_phi);
F1_y_L=S1_Y0+S1_a*cos(F1_theta_L_array)*sin(S1_phi) + ...
            S1_b*sin(F1_theta_L_array)*cos(S1_phi);
F2_x_L=S2_X0+S2_a*cos(F2_theta_L_array)*cos(S2_phi) + ...
            S2_b*sin(F2_theta_L_array)*-sin(S2_phi);
F2_y_L=S2_Y0+S2_a*cos(F2_theta_L_array)*sin(S2_phi) + ...
            S2_b*sin(F2_theta_L_array)*cos(S2_phi);

F1_x_S=S1_X0+S1_a*cos(F1_theta_S_array)*cos(S1_phi) + ...
            S1_b*sin(F1_theta_S_array)*-sin(S1_phi);
F1_y_S=S1_Y0+S1_a*cos(F1_theta_S_array)*sin(S1_phi) + ...
            S1_b*sin(F1_theta_S_array)*cos(S1_phi);
F2_x_S=S2_X0+S2_a*cos(F2_theta_S_array)*cos(S2_phi) + ...
            S2_b*sin(F2_theta_S_array)*-sin(S2_phi);
F2_y_S=S2_Y0+S2_a*cos(F2_theta_S_array)*sin(S2_phi) + ...
            S2_b*sin(F2_theta_S_array)*cos(S2_phi);

S1_middle = [S1_x_data(round(end/2)) S1_y_data(round(end/2))];
S2_middle = [S2_x_data(round(end/2)) S2_y_data(round(end/2))];
```

```
F1_LS_middle = [F1_x_L(round(end/2)) F1_y_L(round(end/2));
                F1_x_S(round(end/2)) F1_y_L(round(end/2))];

F2_LS_middle = [F2_x_L(round(end/2)) F2_y_L(round(end/2));
                F2_x_S(round(end/2)) F2_y_S(round(end/2))];

F1_LS_dist = ((F1_LS_middle(:,1)-S1_middle(1)).^2 + ...
             (F1_LS_middle(:,2)-S1_middle(2)).^2).^(1/2);
F2_LS_dist = ((F2_LS_middle(:,1)-S2_middle(1)).^2 + ...
             (F2_LS_middle(:,2)-S2_middle(2)).^2).^(1/2);

[~,F1_idx]=min(F1_LS_dist);
[~,F2_idx]=min(F2_LS_dist);

if F1_idx==1
    F1_x=F1_x_L;
    F1_y=F1_y_L;
else
    F1_x=F1_x_S;
    F1_y=F1_y_S;
end
if F2_idx==1
    F2_x=F2_x_L;
    F2_y=F2_y_L;
else
    F2_x=F2_x_S;
    F2_y=F2_y_S;
end
```

Plot fits

```
figure
plot(S1_x_data/1000,S1_y_data/1000)
hold on
plot(S2_x_data/1000,S2_y_data/1000)
plot(S3_x_data/1000,S3_y_data/1000)
plot(S4_x_data/1000,S4_y_data/1000)
plot(F1_x/1000,F1_y/1000,'m')
plot(F2_x/1000,F2_y/1000,'m')
plot([I13_x I23_x]/1000,[I13_y I23_y]/1000,'m')
plot([I14_x I24_x]/1000,[I14_y I24_y]/1000,'m')
scatter([I13_x I14_x I23_x I24_x]/1000,[I13_y I14_y I23_y I24_y]/1000,...
       'm','filled')
scatter([F1_x(1) F2_x(1)]/1000,[F1_y(1) F2_y(2)]/1000)
xlabel('Distance from Greenwich Meridian [m]', 'Fontsize', 14)
```

```
ylabel('Distance from Equator [m]', 'Fontsize', 14)
title(sprintf('Clay Plug %d: Imported Google Earth Data + Best Fits', ...
      Plugs(i)),'Fontsize',18)
```

Clay plug surface area calculations

```
% Calculate length dl between ellipses per generated point
dl = sqrt((F1_x-F2_x).^2 + (F1_y-F2_y).^2);
% Calculate averaged dl
dl_1=dl(1:1:end-1);
dl_2=dl(2:1:end);
dl_av=(dl_1+dl_2)/2;

% Calculate width db between two generated points
dw_1 = sqrt( (diff(F1_x)).^2 + (diff(F1_y).^2) ); % inner bend
dw_2 = sqrt( (diff(F2_x)).^2 + (diff(F2_y).^2) ); % outer bend
dw_av = (dw_1+dw_2)/2;

% Calculate area mini rectangles
area_recs = dl_av.*dw_av;

% Total area clay plug
Plug_SurfaceArea(i) = sum(area_recs); % Surface area clay plug in m^2
```

Depth Profile 1

```
% Equal surface area to Profile 2

% Calculate clay plug volume
P1_SurfaceArea = 0.5*Depth*dl_av; % Calculate area of depth profile "slice"
P1_VolumeRec = P1_SurfaceArea.*dw_av; % Calculate volume elements
Plug_Volume_P1(i) = sum(P1_VolumeRec); % Total volume clay plug m^3
```

Depth Profile 3

```
P3_x_DP_Par = Fraction_W*dl_av; % Locations deepest points

P3T_P = ((P3_x_DP_Par.^2)/(4*Depth))-((P3_x_DP_Par.^2)/(2*Depth));
P3T_Q = dl_av-P3_x_DP_Par;
P3T_R = -Depth;
P3T_D = P3T_Q.^2-4*P3T_P*P3T_R;
P3T_C = (-P3T_Q + sqrt(P3T_D))./(2*P3T_P);

P3T_r_SNIJ = (P3T_C.*((P3_x_DP_Par.^2)/(2*Depth))+P3_x_DP_Par);
P3T_z_SNIJ = (Depth./(P3_x_DP_Par.^2)).*(P3T_C.*((P3_x_DP_Par.^2)./ ...
             (2*Depth))).^2-Depth;
```

```
P3T_r_PAR = repmat(linspace(0,1,100)',1,numel(P3T_r_SNIJ)).* ...
            repmat(P3T_r_SNIJ,100,1);
P3T_F_matrix = repmat(P3_x_DP_Par,100,1);
P3T_z_PAR = Depth./(P3T_F_matrix.^2).*(P3T_r_PAR-P3T_F_matrix).^2-Depth;

P3T_r_LIN = ((repmat (linspace(0,1,100)',1, numel(P3T_r_SNIJ))).* ...
            (repmat((dl_av-P3T_r_SNIJ),100,1) )) ...
        + repmat(P3T_r_SNIJ,100,1);
P3T_z_LIN =((repmat(P3T_C,100,1)).*P3T_r_LIN)-repmat((P3T_C.*dl_av),100,1);

P3T_area_zPAR = abs(1/3*Depth./(P3_x_DP_Par.^2).* ...
                (P3T_r_SNIJ-P3_x_DP_Par).^3-Depth*P3T_r_SNIJ- ...
                1/3*Depth./(P3_x_DP_Par.^2).*(-P3_x_DP_Par).^3);
P3T_area_zLIN = abs(0.5.*P3T_z_SNIJ.*(dl_av-P3T_r_SNIJ));

P3_SurfaceArea = P3T_area_zPAR + P3T_area_zLIN; % Calc area depth slice
P3_VolumeRecs = P3_SurfaceArea.*dw_av; % Create volume elements
Plug_Volume_P3(i) = sum(P3_VolumeRecs); % Calculate volume clay plug [m^3]

figure
plot (P3T_r_PAR(:,1:end),P3T_z_PAR(:,1:end))
hold on
plot (P3T_r_LIN(:,1:end),P3T_z_LIN(:,1:end))
```

Calculate Arsenic content

```
% Average grain size distribution from data D. Ghosh (2015)
GS_CoarseSand = 0.066; % percentage of total
GS_FineSand = 0.194;
GS_Silt = 0.395;
GS_Clay = 0.345;
GS_SS = GS_CoarseSand + GS_FineSand + GS_Silt; % Similar initial porosities

% Initial porosity ranges
C_InPor_Min = 0.40; % Initial porosity clay, minimum
C_InPor_Max = 0.95; % Initial porosity clay, maximum
SS_InPor_Min = 0.35; % Initial porosity sand+silt, minimum
SS_InPor_Max = 0.42; % Initial porosity sand+silt, maximum

% Calculate range water content, range clay and range sand+silt
W_Min = C_InPor_Min*GS_Clay + SS_InPor_Min*GS_SS; % Min water % of total
W_Max = C_InPor_Max*GS_Clay + SS_InPor_Max*GS_SS; % Max water % of total
C_Min = (1-C_InPor_Max)*GS_Clay; % Min. clay content
C_Max = (1-C_InPor_Min)*GS_Clay; % Max. clay content
SS_Min = (1-SS_InPor_Max)*GS_SS; % Min. sand+silt content
```

```
SS_Max = (1-SS_InPor_Min)*GS_SS; % Max. sand+silt content

% Calculate specific weight range and weight of clay plug
Rho_W = 1000; % Density water [kg/m^3]
Rho_Illite = 2740; % Average density illite
Rho_Montmo = 1850; % Average density montmorillonite
Rho_Kao = 2600; % Density kaolinite
Rho_C = (Rho_Illite+Rho_Montmo+Rho_Kao)/3; % Average density clay particles
Rho_Q = 2650; % Density quartz

Rho_Min = (C_Min*Rho_C) + (SS_Min*Rho_Q) + (W_Max*Rho_W); % kg/m3
Rho_Max = (C_Max*Rho_C) + (SS_Max*Rho_Q) + (W_Min*Rho_W);

Plug_Weight(1,i) = Rho_Min*Plug_Volume_P3(i);
Plug_Weight(2,i) = Rho_Max*Plug_Volume_P3(i);

% Calculate Arsenic content
AS = ((21.2+14.2)/2)/1000; % g Arsenic / kg sediment (Upper 12 meters)
% From (D. Ghosh, 2015)

Plug_As(1,i) = (AS*Plug_Weight(1,i))/1000; % Min. kg As in clay plug
Plug_As(2,i) = (AS*Plug_Weight(2,i))/1000; % Max. kg As in clay plug
```

Flux Estimations

```
% Calculate contact area between Clay plug and adjecent Point Bar
P3_x_DP_Lin = (1-Fraction_W)*dl_av; % Locations deepest points
ds_av = sqrt( Depth^2 + P3_x_DP_Lin.^2); % Calculate av length along slope
area_SlopeRecs = ds_av.*dw_av; % Calculate surface elements
Plug_ContactArea(i) = sum(area_SlopeRecs); %Contact area CP & PB  [m^2]

% Calculate the flux (Ficks 1st Law modified for membrames)
W_Vol(1,i) = W_Min * Plug_Volume_P3(i); % Min. water volume
W_Vol(2,i) = W_Max * Plug_Volume_P3(i); % Max. water volume

% Caluclate the As Concentration
AS_Conc(1,i) = (Plug_As(1,i)/W_Vol(2,i)) * Fraction_Diss;
AS_Conc(2,i) = Plug_As(2,i) / W_Vol(1,i) * Fraction_Diss;

% Calculation the initial diffusion flux
Plug_Flux(1,i) = HC_Min * AS_Conc(1,i)*3600*24*365*1000; % Min. (Initial)
                                                %Flux to point bar [g/m^2 year]
Plug_Flux(2,i) = HC_Max * AS_Conc(2,1)*3600*24*365*1000; % Max. Flux
                                                    %to point bar [g/m^2 year]

% Initial discharge kg/day
```

```
Plug_Q(1,i) = Plug_Flux(1,i)*Plug_ContactArea(i)/1000/365;
Plug_Q(2,i) = Plug_Flux(2,i)*Plug_ContactArea(i)/1000/365;

end
```

Plot Histogram

```
% Plot histrogram of clay plug volumes
figure
hist(Plug_Volume_P3)
xlabel('Volume Clay Plug [m^3]', 'Fontsize', 14)
ylabel('Frequency', 'Fontsize', 14)
title('Histogram Clay Plug Volumes','Fontsize',18)
```